Technical Report Documentation Page

1. Report No. ABC-UTC-2016-C5-UW01-Final	2. Government Accession No.	3. Recipient's Catalog No.	
4. Title and Subtitle **Exploring the Combined Use of Distributed Fiber and Deformed Bar Reinforcement to Resist Shear Forces**		5. Report Date May 2024 6. Performing Organization Code	
7. Author(s) Benedikt Farag, John Paul Gaston, Paolo M. Calvi (https://orcid.org/0000-0002-0051-2677), and Travis Thonstad (https://orcid.org/0000-0002-1575-3617)		8. Performing Organization Report No.	
9. Performing Organization Name and Address Department of Civil and Environmental Engineering University of Washington, Box 352700 Seattle, WA 98195-2700		10. Work Unit No. (TRAIS) 11. Contract or Grant No. 69A3551747121	
12. Sponsoring Organization Name and Address Accelerated Bridge Construction University Transportation Center Florida International University 10555 W. Flagler Street, EC 3680 Miami, FL 33174 US Department of Transportation Office of the Assistant Secretary for Research and Technology And Federal Highway Administration 1200 New Jersey Avenue, SE Washington, DC 201590		13. Type of Report and Period Covered Final Report (January 2022- May 2024) 14. Sponsoring Agency Code	
15. Supplementary Notes Visit www.abc-utc.fiu.edu for other ABC reports.			
16. Abstract Macro-synthetic fibers are commonly added to concrete mixtures as secondary reinforcement to control temperature and shrinkage cracks in concrete flatwork. The fibers also improve the tensile behavior of the material, however, the contribution of macro-synthetic fibers towards the strength of structural elements is generally neglected. To investigate the influence of macro-synthetic fibers on the shear strength of concrete elements, an experimental and numerical study was performed investigating macro-synthetic fiber-reinforced concrete (PFRC) panels subjected to pure shear loading. Twelve PFRC panel elements were tested under pure shear and were used to calibrate a finite element modeling approach to explore combinations of parameters that were not, or could not be, tested experimentally. The modeling approach was validated against a database of PFRC beams from the literature and used to conduct a parametric study, exploring over 250 combinations of fiber dosage, transverse reinforcement ratio, and concrete compressive strength. The ability of existing empirical equations in model codes to predict the shear strength of PFRC structural elements was also evaluated. The results of the experiments and parametric study indicated that macro-synthetic fibers effectively reduced crack widths and enhanced shear strength, depending on the transverse reinforcement ratio and fiber content. Greater benefits were observed for lower transverse reinforcement ratios (< 0.25%) and higher fiber contents (>1%), exhibiting slightly different trends for the different concrete compressive strengths. The shear strength prediction equations in the AASHTO LFRD Bridge Design Specifications were generally conservative and could be used without modification for PFRC elements with fiber volumes less than 0.5%. For macro-synthetic fiber volume fractions greater than 1.0%, the prediction equations may be overly conservative, although further testing is needed to confirm this assertion.			
17. Key Words fiber-reinforced concrete, macro-synthetic fibers, shear strength, panel test, finite element model		18. Distribution Statement No restrictions.	
19. Security Classification (of this report) Unclassified.	20. Security Classification (of this page) Unclassified.	21. No. of Pages 58	22. Price

Form DOT F 1700.7 (8-72) Reproduction of completed page authorized

(this page is intentionally left blank)

Exploring the Combined Use of Distributed Fiber and Deformed Bar Reinforcement to Resist Shear Forces

Final Report

May 2024

Principal Investigator(s): Travis Thonstad, Paolo M. Calvi

Department of Civil and Environmental Engineering
Florida International University

Authors
Benedikt Farag, John Paul Gaston, Paolo M. Calvi, Travis Thonstad

Sponsored by
Accelerated Bridge Construction University Transportation Center

ACCELERATED BRIDGE CONSTRUCTION
UNIVERSITY TRANSPORTATION CENTER

A report from
Department of Civil and Environmental Engineering
Florida International University
10555 West Flagler Street, EC 3680
Miami, FL 33174
Phone: 305-348-2824 / Fax: 305-348-2802
https://cee.fiu.edu/

DISCLAIMER

The contents of this report reflect the views of the authors, who are responsible for the facts and the accuracy of the information presented herein. This document is disseminated in the interest of information exchange. The report is funded, partially or entirely, by a grant from the U.S. Department of Transportation's University Transportation Program. However, the U.S. Government assumes no liability for the contents or use thereof.

CONTENTS

LIST OF FIGURES

LIST OF TABLES

ACKNOWLEDGMENTS

This project was supported by the Accelerated Bridge Construction University Transportation Center (ABC-UTC at www.abc-utc.fiu.edu) at Florida International University (FIU), as lead institution, and Iowa State University (ISU), the University of Nevada-Reno (UNR), University of Washington (UW), and Oklahoma University (OU) as partner institutions. The authors would like to acknowledge the ABC-UTC support.

The authors would like to extend special appreciation to the ABC-UTC and the U.S. Department of Transportation Office of the Assistant Secretary for Research and Technology for funding this project.

CHAPTER 1. INTRODUCTION

1.1. Project Motivation

Macro-synthetic fibers are often added to concrete mixtures as secondary reinforcement, designed to control shrinkage and temperature cracks and improve the durability of bridge superstructures. The addition of fibers to concrete improves the tensile behavior of the material, which leads to more durable concrete elements with increased ductility and better crack control. In addition to these desirable effects, the tensile strength of the fibers also contributes to the strength of the member, however this benefit is not included in current bridge design specifications [e.g., AASHTO 2020]. The lack of provisions regarding the use of macro-synthetic fibers as supplemental reinforcement is of detriment to the bridge construction industry because the use of fibers in PBEs and cast-in-place connections would result in a reduction of bar reinforcement and congestion, lighter members, smaller crack sizes, better distribution of localized stresses, and increased confinement and performance of member ends. To realize the full benefits of macro-synthetic polyolefin fiber-reinforced concrete (PFRC), additional experimental data and rational design guidelines are needed to predict the shear strength of members containing both macro-synthetic fibers and deformed bar reinforcement.

Previous experiments have studied the influence of concrete strength, fiber type, fiber percentage by volume, fiber aspect ratio, and longitudinal reinforcement ratio on the strength and deformability of fiber reinforced concrete (FRC) beams [e.g., Lantsoght 2019, Shah & Rangan 1971, Mansur et al. 1986, Swamy & Bahia 1985, Li et al. 1992]. These tests have generally focused on steel fiber-reinforced concrete (SFRC) beams without stirrups and with fiber volumes in the range of 2%-4%, as shown by the grey bars in Figure 1-1 [data from Lantsoght 2019]. This is in contrast to current practice, where deformed bars alone are designed to carry the necessary forces and fiber addition rates are often less than 1%. Experimental data on the simultaneous use of deformed bars and distributed fiber reinforcement to provide shear strength is limited [e.g., Swamy & Bahia 1985, Amin & Foster 2015, Cucchiara et al. 2004, Aoude et al. 2012], but the existing evidence suggests that the addition of fibers to beams with deformed bar reinforcement improves the shear strength of the beams and can shift failure from brittle to ductile modes. While this limited test data suggests potential benefits of using fibers as supplemental reinforcement, the interactions and synergies between distributed fiber and deformed bar reinforcement in resisting shear is not well understood.

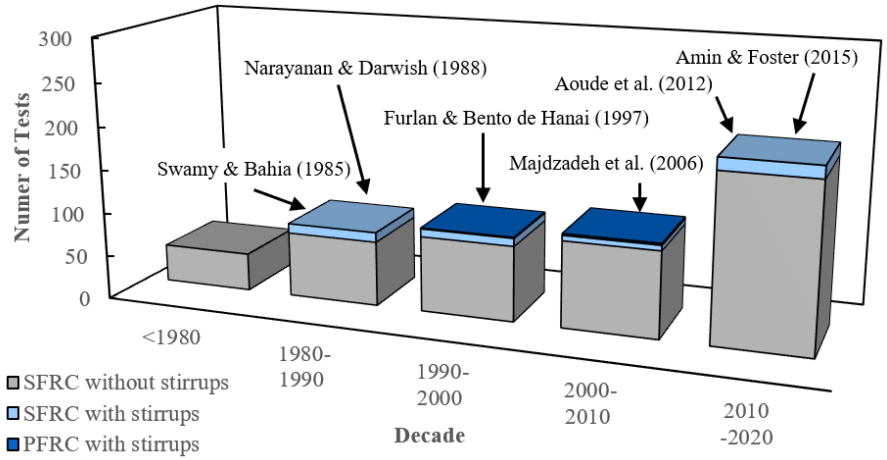

Figure 1-1. Experimental tests of FRC beams, data from [Lantsoght 2019]

Developments in FRCs are applicable to ABC in two ways. The use of FRC would permit thinner prefabricated bridge element (PBE) sections, enabling lighter members for transportation and erection. The great majority of ABC is conducted using PBEs, so any activity that benefits PBEs will encourage the use of them, and by direct implication, ABC. For prestressed girders, the use of FRC could ameliorate the impacts of thinner girder webs by providing additional web-shear cracking strength, by arresting flexural cracks prior to their development into flexure-shear cracks, and by preventing splitting that would be exacerbated by the reduction in web width, as demonstrated in previous test series of girder end regions [e.g., Haroon et al. 2006]. The improved serviceability and durability of prestressed girders made from FRC would also create an additional incentive for owners to choose ABC techniques over other alternatives. Finally, the use of field-cast FRC in ABC projects in connection regions could be beneficial by expediting on-site activities, alleviating congestion in connection regions and reducing the required deformed bar reinforcement.

1.2. Research, Objectives, and Tasks

The objective of the research was the evaluation of existing shear strength prediction equations [e.g., AASHTO 2020] for macro-synthetic fiber reinforced concrete members that also contained deformed bar shear reinforcement. Existing empirical equations for estimating the shear strength of fiber-reinforced concrete elements were evaluated using the experimental response of PFRC panel elements, PFRC beam specimens, and calibrated finite element models. The project included four tasks to achieve the stated research objective:

- *Task 1 – Literature review:* An extensive review of past experimental research involving fiber-reinforced concrete was completed, focusing on specimens that utilized deformed bar and macro-synthetic fiber reinforcement to resist shear forces.
- *Task 2 – Panel testing program:* An experimental panel testing program was completed investigating the interaction between distributed fiber and deformed bar reinforcement in resisting shear forces.
- *Task 3 – Code evaluation:* Using the results of the panel testing program and data is the existing literature, finite element models of PFRC elements were calibrated. Empirical equations for estimating the shear strength of fiber-reinforced concrete elements were then evaluated using the experimental response of PFRC panel elements, PFRC beam specimens, and calibrated finite element models.
- *Task 4 – Final Report*: A final report will be prepared meeting the RITA requirements for UTC funded projects. The content of the report will contain a detailed summary of the results from the preceding tasks and a recommendation for future phases of the project, if necessary.

1.3. Report Overview

The report is organized as follows:

- **Chapter 2. Literature Review:** summarizes past experiments conducted on macro-synthetic fiber-reinforced concrete structural elements, focusing on specimens that utilized deformed bar and macro-synthetic fiber reinforcement to resist shear forces.
- **Chapter 3. Panel Testing Program:** explains the experimental design, specimen

geometry, and specimen parameters used in the panel testing program and summarizes the results of the experiments through tables, plots, and photos.

- **Chapter 4. Finite Element Modeling:** describes the development, calibration, and validation of a finite element modeling approach for PFRC elements using the finite element software VecTor2. This modeling approach was then used to perform a parametric investigation, extending the experimental results.
- **Chapter 5. Comparison with Empirical Shear Strength Equations:** describes empirical shear strength equations available in several model codes and compares the experimental and numerical results to these estimates.
- **Chapter 6. Summary, Conclusions, and Future Work:** summarizes the completed work, draws conclusions based on the results of the study, and presents recommendations for future work.

CHAPTER 2. LITERATURE REVIEW

An extensive search for past experimental research involving polyolefin fiber-reinforced concrete was conducted, focusing on structural specimens that utilized both deformed bar and fiber reinforcement to resist shear forces.

Table 2-1 reviews pertinent experimental tests investigating macro-synthetic fiber-reinforced concrete structural elements, both with and without transverse deformed bar reinforcement. Based on the results of these tests, it was observed that:

- macro-synthetic fibers improve ductility and reduce crack widths in beam specimens, somewhat proportionally to the employed fiber volume [Altoubat et al., 2009];
- in the absence of transverse reinforcement, the addition of macro-synthetic fiber reinforcement can increase the load capacity and ductility of beams by roughly 20-30% when compared to plain reinforced concrete specimens [Altoubat et al., 2009];
- fiber volumes over 1% can negatively affect workability, leading to consolidation issues and reduced strength [Carnovale and Vecchio, 2014]; and
- Beams with both stirrups and macro-synthetic fibers have higher strengths than beams containing only stirrups, and the increase is larger than expected given the resistance of the beams tested with only fibers or stirrups alone [Majdzadeh et al., 2006].

Table 2-1. Structural tests of PFRC elements with and without transverse deformed bar reinforcement

Author	Test	Specimen	Fiber Length (mm)	Fiber Aspect Ratio	Fiber Modulus (GPa)	Fiber Geometry	Fiber volume	Conventional reinforcement	Key conclusions
Li et al. 1992	Flexure /Shear	Beams	12.7	334	100	Straight	V_f = 1.0%	ρ_ℓ = 1.1% / 2.2% ρ_v = 0%	Strength increased between 100-200% when a 1% volume fraction of fibers was used. Possible to obtain ductile flextural failures for variety of reinforcement and span-to-depth ratios.
Li et al. 1994	Shear	Ohno shear beams	12.7	334	100	Straight	V_f = 2.0%	ρ_ℓ = 0% / 0.75% ρ_v = 0% / 0.75%	Fiber reinforced beam exhibted higher shear strenth than plain concrete specimen and lower strength than reinforced one Fibers did not improve first cracking load. Fiber reinforced specimen had improved ultimate strain over beam with conventional concrete and welded wire fabric reinforcement.
Furlan and Bento de Hanai 1997	Flexure /Shear	Beams	42	840		Multi-filament	V_f = 0% / 0.50%	ρ_ℓ = 1.58% ρ_v = 0.18%	Addition of fibers increased stiffness, improved ductility, increased the shear strength, and led to the formation of multiple cracks at failure in the beams Addition of fibers modified the failure mode of the beams from shear to flexure in the presence of stirrups.
Majdzadeh et al. 2006	Flexure /Shear	Beams	50 54	85 360	9.5 3.5	Straight Self-fibrillating	V_f = 0% / 0.5% / 1.0% / 1.5%	ρ_ℓ = 2.62% ρ_v = 0% / 0.14%	Fiber reinforcement enhanced the capacity of the beams. No benefits were noted when the volume fraction was increased beyond 1%. Beams with both stirrups and fibers had higher strengths than beams containing only stirrups, and the increase was larger than expected given the resistance of the beams tested with only fibers or stirrups alone.

Author	Test	Specimen	Fiber Length (mm)	Fiber Aspect Ratio	Fiber Modulus (GPa)	Fiber Geometry	Fiber volume	Conventional reinforcement	Key conclusions
Roesler et al. 2006	Out-of-plane shear	Slabs on grade	40	90	9.5	Straight	V_f = 0% / 0.32% / 0.48%	ρ_ℓ = 0% ρ_v = 0%	Flexural cracking load and strength increased by roughly 30% with addition of fibers The fibers did not increase the tensile capacity of the concrete slabs. Instead, a larger percentage of the fiber reinforced concrete slabs remained in contact with the ground throughout testing, leading to improved capacity.
Altoubat et al. 2009	Flexure /Shear	Beams	40	90	9.5	Straight	V_f = 0% / 0.5% / 0.75% / 1.0%	ρ_ℓ = 2.15% / 3.18% ρ_v = 0%	Addition of fibers increased first diagonal cracking strength and ultimate strength roughly of 20-30% Beam response with fibers was more ductile than control RC beams Fibers changed the cracking pattern and mode of failure of the beams. The fiber-reinforced beams exhibited multiple diagonal cracks before failure occurred. Fibers did not change the load at which the diagonal cracks initiated but did slow down propagation and widening
Carnovale and Vecchio 2014	Shear	Panel element	54	67	10	Crimped	V_f = 0% / 2.0%	ρ_ℓ = 3.31% ρ_v = 0% / 0.42%	First cracking of PFRC panels was accompanied by a sharp drop in load and development of large crack widths Addition of fibers improved ductility, polyolefin fibers can transmit relatively high tensile stress across crack widths No degradation in properties under cyclic loads was observed for macro-synthetic fiber-reinforced panels
Conforti et al. 2015	Flexure /Shear	Beams	50	85	9.5	Straight	V_f = 0% / 0.5% / 1.0 % / 1.5 %	ρ_ℓ = 2.62% ρ_v = 0% / 0.28%	Fibers shifted the failure mode from shear to flexure Fibers at addition rate Vf = 1.45% can completely substitute minimum shear reinforcement Fibers reduced crack with and resulted in a crack spacing reduction of about 40%

Author	Test	Specimen	Fiber Length (mm)	Fiber Aspect Ratio	Fiber Modulus (GPa)	Fiber Geometry	Fiber volume	Conventional reinforcement	Key conclusions
Alhassan et al. 2017	Flexure /Shear	Beams	40	90	9.5	Straight	V_f = 0% / 0.33% / 0.55% / 0.77%	ρ_ℓ = 1.26% / 1.81% / 2.46% / 3.22% ρ_v = 3.33%	Slight increase in strength: roughly 20% increase in strength for a fiber volume fraction of 0.77% Initial, service, and post-cracking stiffness increased with fiber volume fraction
Arslan et al. 2017	Flexure /Shear	Beams	39	50		Straight	V_f = 0% / 1.0% / 2.0 % / 3.0 %	ρ_ℓ = 1.28% ρ_v = 0%	Fibers increased shear strength and ductility Fibers were not capable of shifting the failure mode from shear to flexure for span-to-depth ratios ≤ 3.5 Maximum normalized shear stress increased with increasing fiber addition rates
Navas et al. 2018	Shear friction	Push off (pre-cracked)	48	57	4.7	Crimped	V_f = 0% / 1.1% /	ρ_{vf} = 0%, 0.16%	Initial crack opening influenced stiffness and strength of fiber reinforced specimens less than unreinforced ones Addition of fibers increased shear and normal stresses transferred across the crack

Author	Test	Specimen	Fiber Length (mm)	Fiber Aspect Ratio	Fiber Modulus (GPa)	Fiber Geometry	Fiber volume	Conventional reinforcement	Key conclusions
Patil et al. 2020	Flexure /Shear	Columns	50	100	10	Deformed	V_f = 0% / 0.35% / 0.7% / 1.0%	ρ_ℓ = 0.84% GFRP ρ_v = 0.35% GFRP	Addition of fibers improved post-cracking stiffness of beams Fibers caused a marginal increase in peak strength

CHAPTER 3. PANEL TESTING PROGRAM

The objective of the experimental test program was to elucidate the contributions and benefits of the separate and combined use of deformed bar and macro-synthetic fiber reinforcement. Previous tests of PFRC members did not include deformed bar reinforcement or included only a single deformed bar reinforcement configuration (e.g., ρ_v = 0.14% for the beams tested by Majdzadeh et al. 2006). This was one of the first experimental programs to specifically investigate the interaction between macro-synthetic fibers and deformed bar reinforcement in resisting shear forces and provides valuable test data. Additional details about the test program can be found in Gaston (2023).

3.1. Experimental Matrix

Table 3-1 summarizes properties of the panel specimens that were constructed and tested. The variables of interest within the experimental campaign included the deformed bar and macro-synthetic fiber reinforcement ratios, expressed as V_f the fiber volume fraction (fiber volume / total volume), and ρ_v the transverse reinforcement ratio (area of deformed bar / thickness of element × bar spacing). A 3×4 full factorial experimental design was selected to enable the quantification of interactions between the primary variables and ample coverage of the region of interest. The selected fiber volume fractions were consistent with what is currently used in practice and recommended by the manufacturer.

Table 3-1. Panel testing program specimen properties

Specimen name			Concrete	Elastic	4×4 Beams		6×6 Beams	
	V_f (%)	ρ_v (%)	strength (psi)	modulus (ksi)	Peak, f_1 (psi)	Residual, f_{150} (psi)	Peak, f_1 (psi)	Residual, f_{150} (psi)
PFRC-000-000	0	0	6400	4700	750			
PFRC-000-029	0	0.29	5500	4100	850		790	
PFRC-000-058	0	0.58	4500	4300	440			
PFRC-000-114	0	1.14	6100	4700	770		650	
PFRC-026-000	0.26	0	4700	3800	710	70	860	100
PFRC-026-029	0.26	0.29	5500	4400	730	150	630	140
PFRC-026-058	0.26	0.58	5000	3900	780	60	700	90
PFRC-026-114	0.26	1.14	6300	4600	710	60	560	100
PFRC-052-000	0.52	0	4300	*	590	140	530	170
PFRC-052-029	0.52	0.29	6500	4300	790	180	630	200
PFRC-052-058	0.52	0.58	5100	4700	560	120	630	110
PFRC-052-114	0.52	1.14	5200	4100	660	180	500	190

* Elastic modulus not available due to instrument malfunction during testing

3.2. Reinforcement

Figure 3-1 shows the reinforcement layouts for the panel specimens. All reinforcement for the project was No. 3 A706 Gr 60 [ASTM 2022] from the same heat (with a yield stress of 74.3 ksi and ultimate stress of 101.2 ksi). For all configurations, the longitudinal reinforcement ratio was held constant at ρ_ℓ = 2.28%. This reinforcement ratio was selected to force failure in the transverse direction and was based on previous experience with similarly reinforced specimens tested with the panel tester [e.g., Zhang et al. 2020]. In the transverse direction, the spacing of

the continuous reinforcement varied between panels, from ρ_y = 0.29% to ρ_y =1.14%, with three unreinforced specimens (ρ_y = 0%) acting as benchmarks.

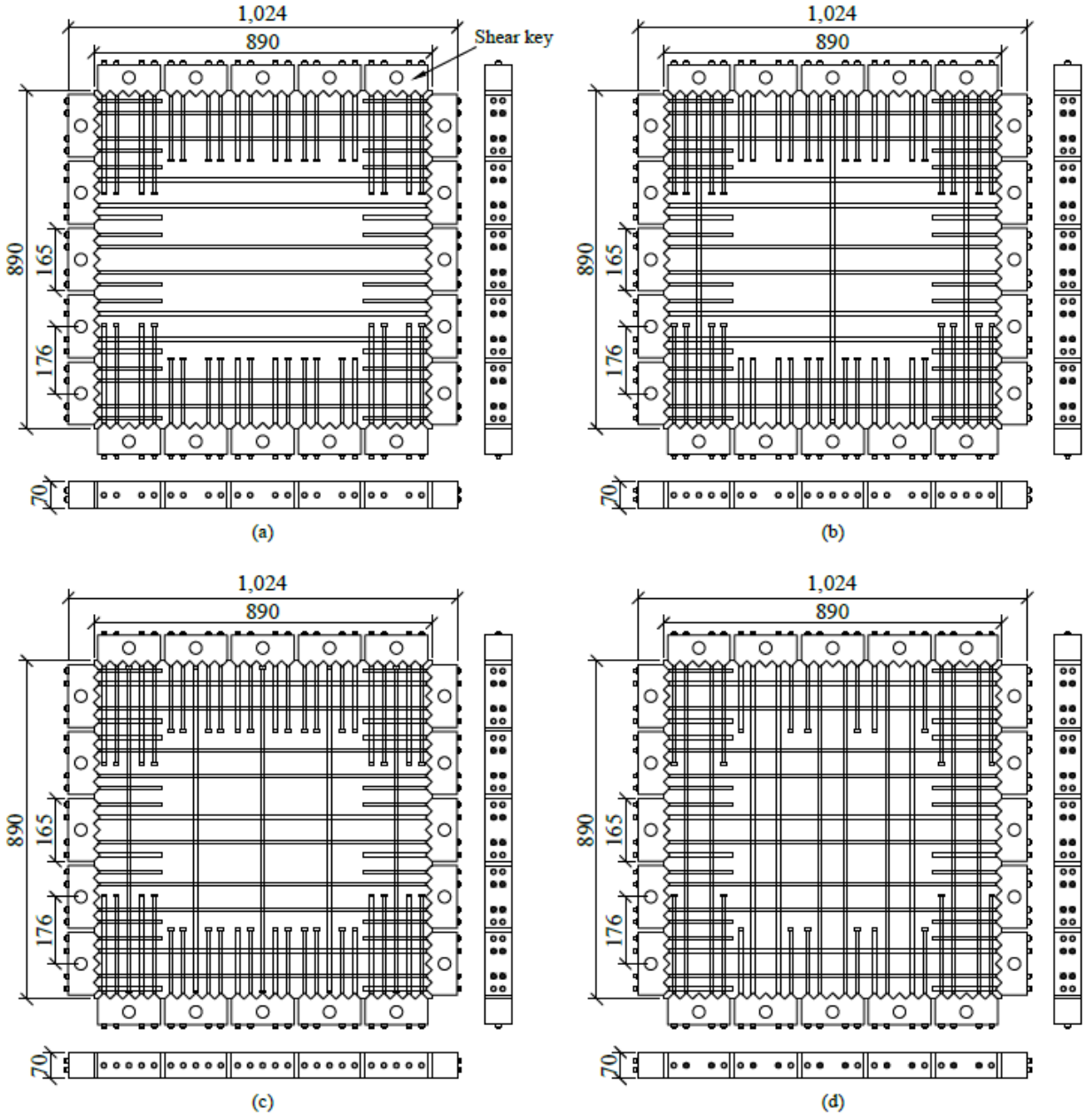

Figure 3-1. Reinforcement layout (ρ_t = 2.28% for all configurations) (a) ρ_y = 0%, (b) ρ_y = 0.29%, (c) ρ_y = 0.58%, and (d) ρ_y = 1.14% (Note: 1 mm = 0.039 in)

The macro-synthetic fibers that were used for the panel specimens, STRUX 90/40, were manufactured by GCP Applied Technologies. The fibers were rectangular in cross section with a length of 1.55 in and equivalent aspect ratio of 90. The virgin polypropylene and polyethylene blend fibers used in this experimental program were from the same lot. These fibers were selected due to their high modulus (1390 ksi) and successful use in a number of previous tests of

structural members [e.g., Altoubat et al. 2009]. The fibers comply with ASTM D7508 [ASTM 2020b] and have been evaluated by the ICC (ESR-2942).

3.3. Concrete

Table 3-2 gives the concrete mixture proportions for the panel specimens. To accommodate wetting the surface area of the macro-synthetic fibers, the mixture design without fibers (M1) for panels was modified by replacing three fiber volumes of fine aggregate with one fiber volume of fibers and two fiber volumes of coarse aggregates (M2 and M3). The original mixture design was selected in coordination with a regional ready mixed concrete supplier, who donated the aggregate from their aggregate plant in Dupont, WA. The fine aggregate was washed building sand, conforming to ASTM C33 [ASTM 2023], and the coarse aggregate was washed 3/8 in gravel, conforming to ASTM C33 No. 8 [ASTM 2023]. Selecting a commercially available concrete mixture and procuring aggregate from their plant was advantageous to ensure that the research results were consistent and scalable.

Table 3-2. Concrete mixture design for panel specimens (SSD weight)

Constituent	Absorp (%)	Specific Gravity	M1 0% fibers (lb/yd^3) *	M2 0.25 % fibers (lb/yd^3)*	M3 0.52% fibers (lb/yd^3)*
Cement (IL)		3.15	534	534	534
Fine Aggregate	2.10	2.65	1447	1413	1380
Coarse Aggregate	1.12	2.68	1815	1838	1860
Water			267	267	267
Air (1.5%)					
Fibers		0.92	0	4	8
Total			4062	4059	4056

*WRDA64 and ADVA195 dosage rates for all three mixes are in the range of 3-25 fl. oz / yd^3

Table 3-1 gives a summary of the measured material properties on testing day for the tested panels. To accompany the panel elements, 4×8 cylinders and ASTM C1609 [ASTM 2020] beams were cast at the same time as the panel elements. These companion specimens were used to determine strength and toughness parameters needed to calibrate finite element models.

3.4. Test Setup

Figure 3-2 shows a schematic of the UW SETL Panel Element Tester, an advanced apparatus that can apply any combination of in-plane stresses to planar reinforced concrete elements. The panel specimens, 35 in × 35 in × 2.75 in, were connected to the Panel Element Tester through "toothed" anchor blocks affixed to the concrete panel. Each deformed bar embedded in the panel concrete was threaded at its ends, passed through the steel anchor blocks, and anchored to the blocks using nuts. The anchor blocks connected to the Panel Element Tester through 20 vertical and 20 horizontal links. Of these 40 links, 37 were connected to 60 kip hydraulic actuators (blue and green arrows in Figure 3-8) and 3 were fixed (yellow rectangles in Figure 3-8) to act as supports. Forces from the actuators were resisted by a stiff reaction frame and a restraint system on the back side of the panel, between the anchor blocks and the rigid frame, prevented out-of-plane movement. Pressure transducers were used to measure forces produced by the actuators.

The deformations in the panels were monitored using non-contact instrumentation and affixed displacement transducers.

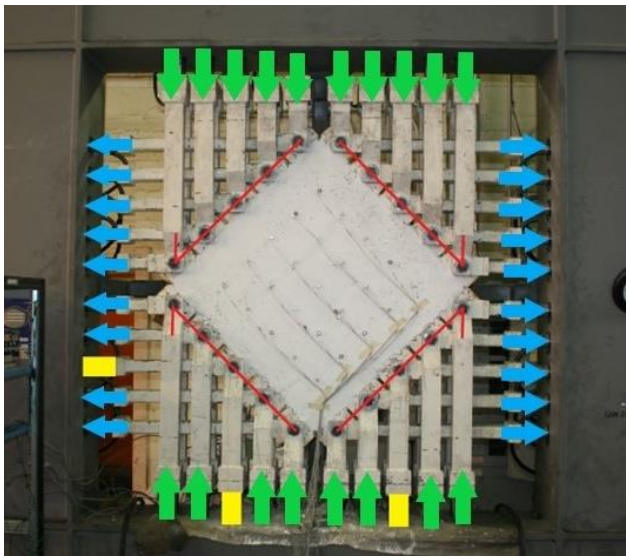

Figure 3-2. Panel Element Tester

Figure 3-3 shows the non-contact instrumentation that was used on the front (bottom casting surface) of the panel specimens. The location of infrared LED targets adhered to the surface of the panel were resolved in three-dimensional space using an OptoTrak camera and corresponding software. The LED targets were placed in a 5×5 grid spaced evenly across the 25.25 in×25.25 in test region (resulting in a 5.3 in × 5.3 in mm grid). The OptoTrak camera was set up directly in front of the panel with good line of sight on all the targets. The output from the system was the x-, y-, and z-coordinates of the targets in the camera's coordinate system, which was collected at a rate of 10 Hz.

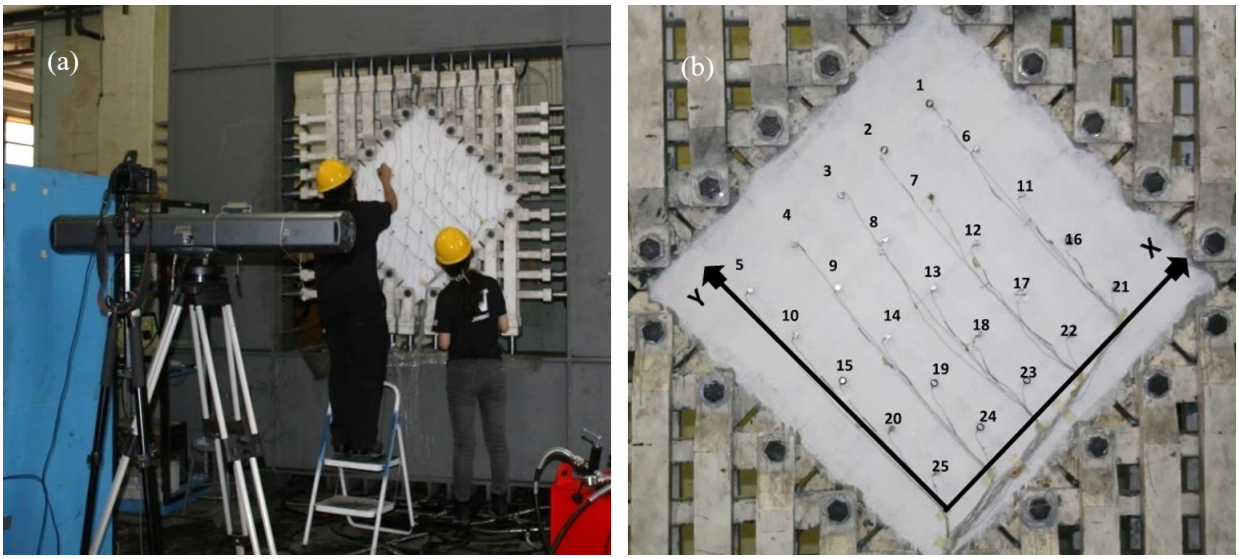

Figure 3-3. Non-contact instrumentation (a) camera setup and (b) LED target layout

3.5. Test Procedure

Figure 3-4 shows, schematically, the shear stress versus time for a typical panel specimen. Shear stresses were applied to the panel slowly, increasing load on the panel until first cracking was achieved. The load was then reduced, by roughly 10% of the cracking load, to limit additional deformation while visible cracks were marked, measured, and photographed. Photos of both the front and back of the panel were also taken. After first cracking, loads were slowly increased in stages until failure with the second pause for crack mapping occurring at a shear stress of 0.313 ksi and all subsequent pauses occurring at 0.104 ksi intervals. Each stage followed the same process of reducing the load and marking, measuring, and photographing visible cracks.

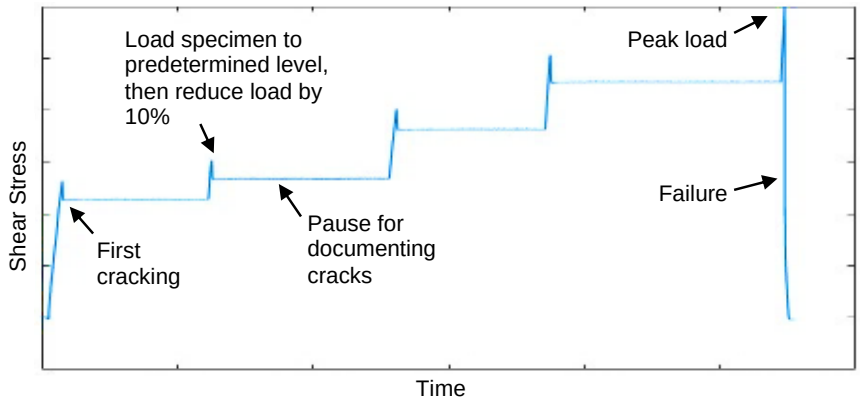

Figure 3-4. Schematic of panel element test procedure

3.6. Normalized Shear Strength

Figure 3-5 shows the normalized shear stress-shear strain behavior for all the panels. To allow comparisons between the tests, the applied shear stress for each panel was normalized by the square root of the average compressive strength of the concrete cylinders tested on the same day as the panel. In general, the panels all had cracking stresses around $0.09\sqrt{f'_c}$ (COV of 0.18) and panels with higher transverse reinforcement ratios exhibited greater shear strengths, as anticipated.

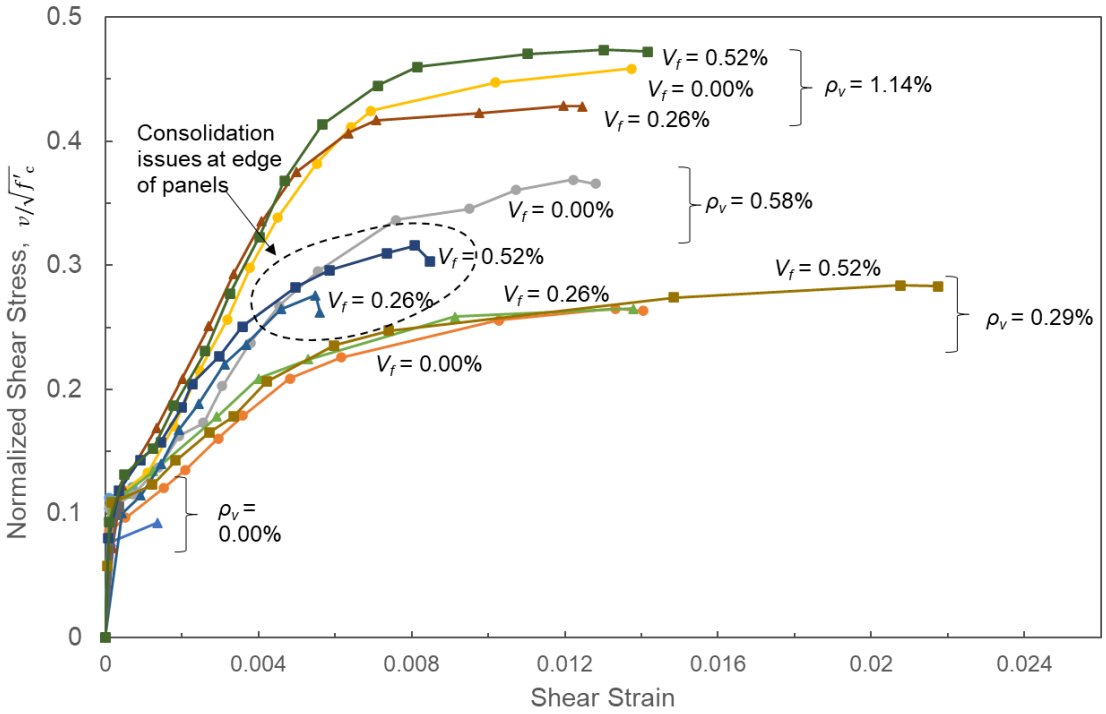

Figure 3-5. Normalized shear stress-shear strain behavior for all panels (f'_c in ksi)

Figure 3-6 shows the normalized shear strength of all twelve panels plotted against the transverse reinforcement ratio and fiber volume ratio. Also shown is the shear strength of the panels estimated using the AASHTO one-way shear strength equations in Section 5.7.3.4 (AASHTO 2020), assuming an angle of inclination of θ = 45, a strength factor β = 2, a transverse yield stress of f_y=74.3 ksi, and a nominal 28-day concrete compressive strength of f'_c=5.4 ksi. The shear strength of the panels increased with increases to the transverse reinforcement ratio, as expected. The increase in strength was consistent with AASHTO estimates for reinforced concrete elements with transverse reinforcement ratios in the range considered in this study. The normalized shear strength did not decrease as the fiber volume increased, regardless of reinforcement level. The main exception was the fiber-reinforced panels with 0.58% transverse reinforcement, which experienced consolidation issues that led to lower strengths.

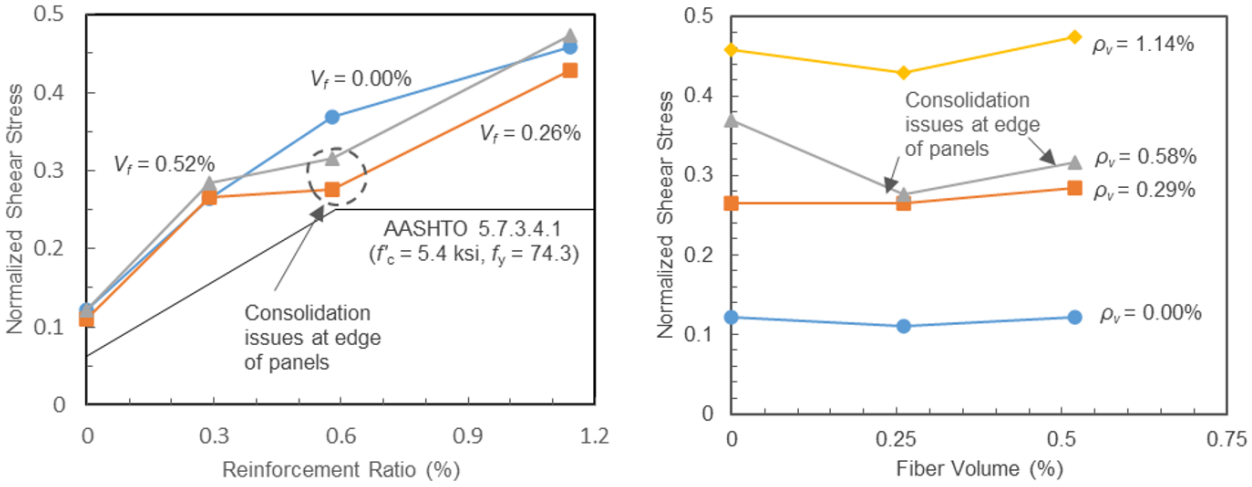

Figure 3-6. Normalized shear strength ($\sqrt{f'c}$ in ksi)

3.7. Observed Damage

Figure 3-7 shows photographs of all twelve panels after failure. The panels without transverse reinforcement failed due to deterioration of aggregate interlock, while the biaxially reinforced panels specimens failed through yielding of the transverse reinforcement.

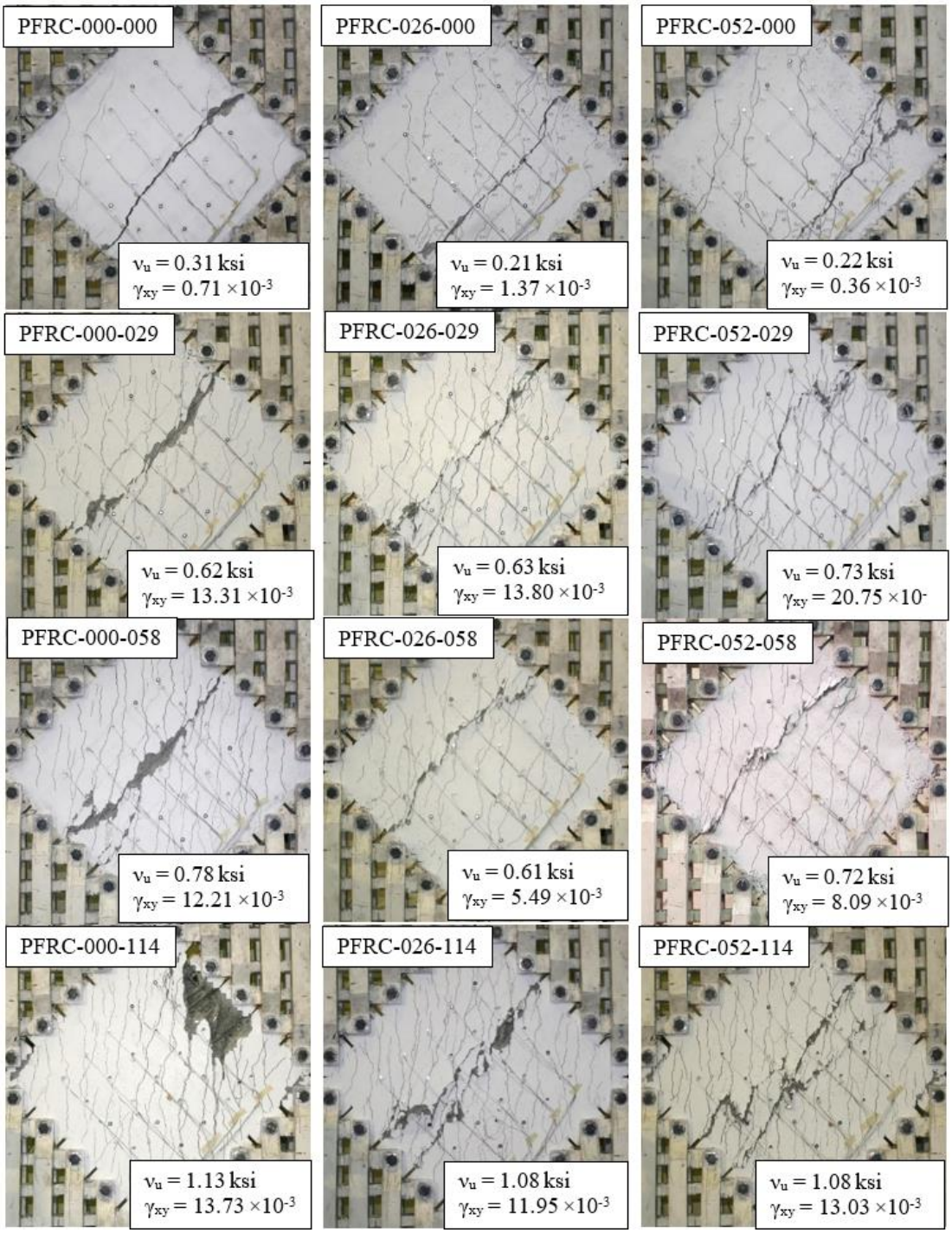

Figure 3-7. Failure patten of tested panel specimens

3.8. Shear Strain at Failure

Figure 3-8 shows the shear strain at failure for all twelve panels plotted against transverse reinforcement ratio and fiber volume ratio. The shear strain at failure increased transitioning from specimens with no shear reinforcement to specimens containing at least the minimum transverse reinforcement required by the AASHTO code (i.e., comparing strain values at 0 and 0.29 transverse reinforcement ratios). The relatively lower maximum shear strain values for the two fiber-reinforced specimens with 0.58% transverse reinforcement, PFRC-026-058 and PFRC-052-058, were attributed to the consolidation issues which occurred in the heavily reinforced edges of those panels that led to premature failure. The influence of fiber volume fraction on the shear strain at failure was found to depend on reinforcement ratio. Panels with 1.14% transverse reinforcement had consistent shear strains at failure despite the addition of fibers. However, at a transverse reinforcement ratio of 0.29%, an increase in shear strain at failure was observed with the addition of macro-synthetic fibers.

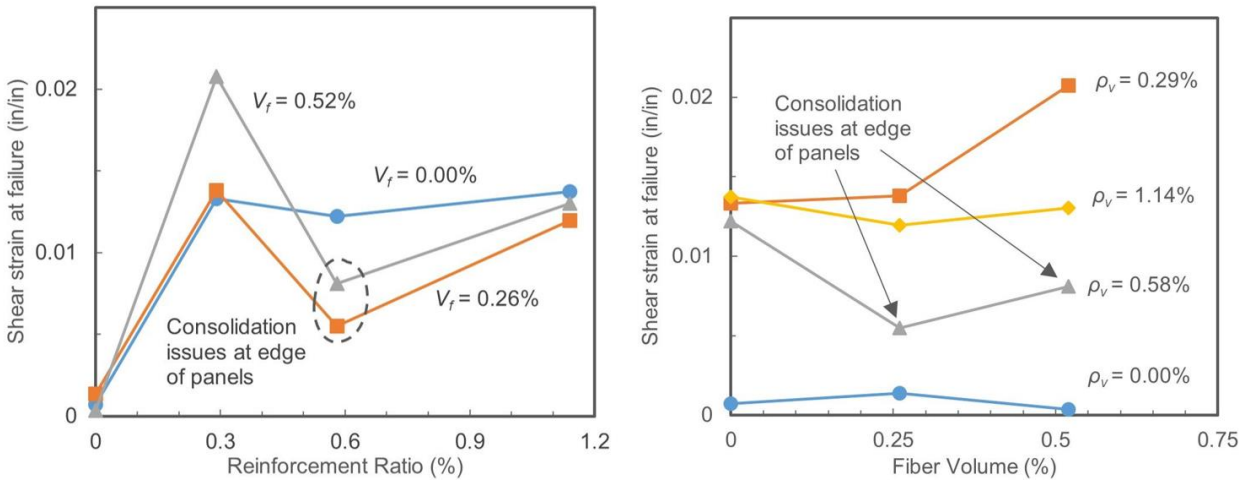

Figure 3-8. Shear strain at failure

3.9. Crack Widths

Figure 3-9 shows the average crack width in each panel at a normalized shear stress of $0.13\sqrt{f'c}$ (ksi) versus the reinforcement ratio and fiber volume fraction. The panels without transverse reinforcement did not reach this shear stress level and are, therefore, not shown in the plot. In general, the average crack width at a normalized shear stress of $0.13\sqrt{f'c}$ (ksi) tended to decrease as the transverse reinforcement ratio and fiber volume fraction increased.

Figure 3-10 shows the maximum crack width at a normalized shear stress of $0.13\sqrt{f'c}$ (ksi) plotted against transverse reinforcement ratio and fiber volume fraction. The panels without transverse reinforcement did not reach this shear stress level and are, therefore, not shown in the plot. In general, the maximum crack width at a normalized shear stress of $0.13\sqrt{f'c}$ (ksi) tended to decrease as either the transverse reinforcement ratio or fiber volume increased.

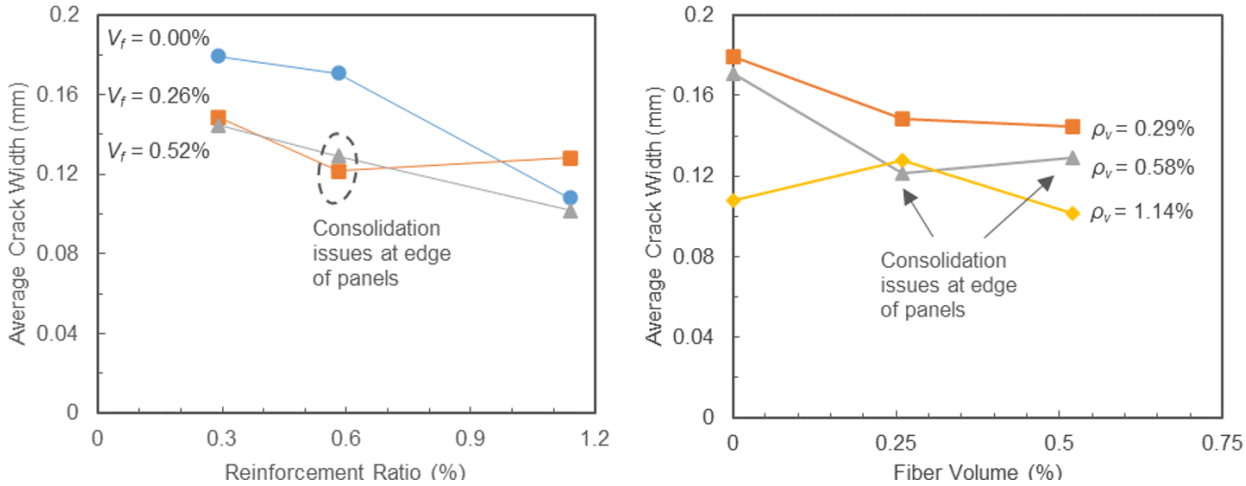

Figure 3-9. Average crack width at a normalized shear stress of $0.13\sqrt{f'c}$

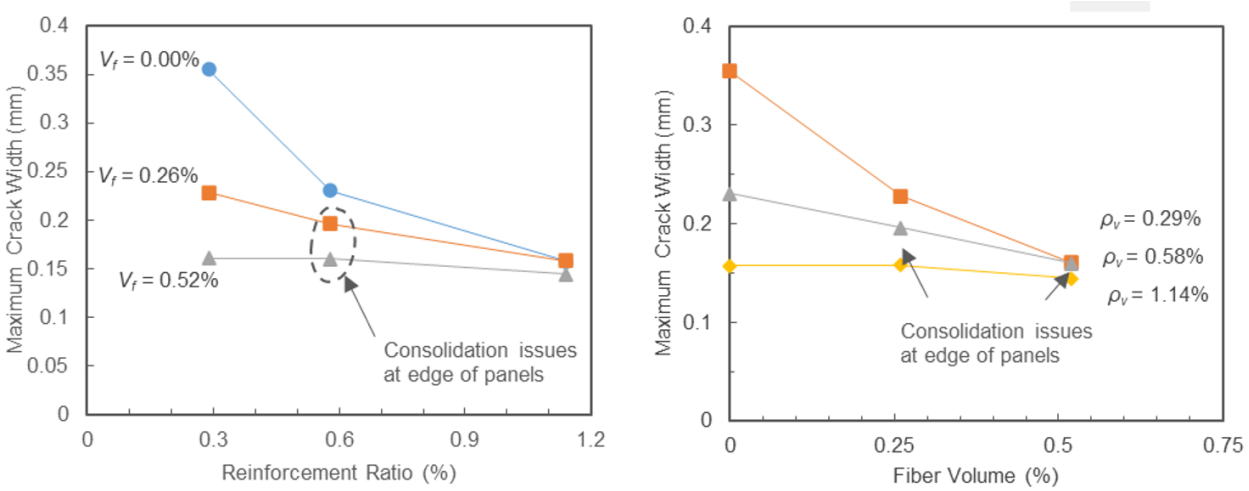

Figure 3-10 Maximum crack width at a normalized shear stress of $0.13\sqrt{f'c}$

3.10. Summary

Table 3-3 summarizes results from the test series including the cracking stress and strain and values of the shear stress, shear strain, concrete principal stresses, concrete principal strains, crack width, and crack spacing at the final load stage before failure for all twelve panels.

The principal stresses and strains in the concrete were estimated from the measured data using equilibrium. For an arbitrary i-direction, the relationship between the normal stress in the steel, f_{si}, the normal stress in the concrete, f_{ci}, and the normal applied stress, f_i, was given by Equation 1.

$$f_i = f_{ci} + \rho_{si} f_{si} \tag{3-1}$$

where ρ_{si} is the reinforcement ratio in the i-direction. Since the tested panels were subjected to pure shear, the applied normal stress in the x- and y-directions were zero, and the stresses in the concrete and steel were related by

$$f_{ci} = -\rho_{si} f_{si} \tag{3-2}$$

To compute the stress in the concrete, the stress in the reinforcement was determined using Equation 3-3, limited to the measured yield stress of the steel f_{sy}, and the measured elastic modulus of the steel, E_s, and the measured strain in the i -direction, ϵ_i.

$$f_{si} = \epsilon_i E_s \leq f_{sy} \tag{3-3}$$

The shear stress in the concrete was assumed to be equal to the applied shear stress, v_{xy}. From these relationships, the principal stresses in the concrete, $f_{c1,2}$, were computed using the stress transformation equation:

$$f_{c1,2} = \frac{f_{cx}+f_{cy}}{2} \pm \sqrt{\left(\frac{f_{cx}-f_{cy}}{2}\right)^2 + (v_{xy})^2} \tag{3-4}$$

where the calculated concrete stresses in the x- and y-directions were given by f_{cx} and f_{cy}, respectively, and the applied shear stress was given by v_{xy}. The principal strain orientation, θ_ε, and magnitude, $\varepsilon_{1,2}$, were also calculated for the panels, in a similar fashion:

$$\varepsilon_{1,2} = \frac{\varepsilon_x+\varepsilon_y}{2} \pm \sqrt{\left(\frac{\varepsilon_x-\varepsilon_y}{2}\right)^2 + (\frac{\gamma_{xy}}{2})^2} \tag{3-5}$$

$$\theta_\varepsilon = \frac{1}{2}\tan^{-1}(\frac{\gamma_{xy}}{\varepsilon_x-\varepsilon_y}) \tag{3-6}$$

Where ε_x and ε_y were the average strains in the test region in the x- and y-directions, and γ_{xy} was the computed average shear strain in the test region.

Table 3-3. Panel Element Test Program Summary

Panel Specimen	f'_c (ksi)	ν_{cr} (ksi)	γ_{cr} (10^{-3})	$f_{c1,max}$ (ksi)	ν_u (ksi)	γ_{xy} (10^{-3})	ε_x (10^{-3})	ε_y (10^{-3})	f_{c1} (ksi)	f_{c2} (ksi)	ε_1 (10^{-3})	ε_2 (10^{-3})	f_{sx} (ksi)	f_{sy} (ksi)	w_m (in)	s_m (in)
PFRC-000-000	6.5	0.29	0.12	0.32	0.31	0.71	0.11	0.42	0.28	-0.3	0.65	-0.13	2.8	-	-	-
PFRC-000-029	5.5	0.20	0.09	0.21	0.62	13.31	2.04	13.74	0.05	-1.5	16.75	-0.97	53.3	74.4	0.021	4.3
PFRC-000-058	4.5	0.23	0.09	0.23	0.78	12.21	2.76	9.72	0.00	-2.0	13.27	-0.79	71.9	74.3	0.020	2.7
PFRC-000-114	6.1	0.28	0.22	0.28	1.13	13.73	4.21	8.35	0.00	-2.5	13.45	-0.89	74.3	74.3	0.013	2.5
PFRC-026-000	4.7	0.17	0.13	0.17	0.21	1.37	0.96	0.37	0.07	-0.6	1.41	-0.08	25.0	-	-	-
PFRC-026-029	5.6	0.26	0.08	0.25	0.63	13.8	1.6	11.05	0.11	-1.3	14.68	-2.03	41.9	74.3	0.012	2.7
PFRC-026-058	5.0	0.23	0.38	0.19	0.61	5.49	1.44	4.45	0.01	-1.3	6.08	-0.18	37.7	74.3	0.010	2.7
PFRC-026-114	6.3	0.26	0.37	0.26	1.08	11.95	2.26	7.92	0.01	-2.2	11.71	-1.52	59.0	74.3	0.016	2.7
PFRC-052-000	4.3	0.20	0.24	0.22	0.22	0.36	0.07	0.18	0.20	-0.2	0.31	-0.06	1.9	-	-	-
PFRC-052-029	6.5	0.26	0.31	0.29	0.73	20.75	2.38	19.75	0.09	-1.8	24.6	-2.46	62.2	75.3	0.019	2.5
PFRC-052-058	5.1	0.26	0.37	0.22	0.72	8.09	2.02	7.04	0.00	-1.6	9.29	-0.23	52.6	74.3	0.012	2.7
PFRC-052-114	5.2	0.27	0.47	0.36	1.08	13.03	2.54	8.52	0.00	-2.3	12.7	-1.63	66.4	74.3	0.017	2.5

CHAPTER 4. FINITE ELEMENT MODELING

Finite element panel models were developed, using the finite element software VecTor2 [Wong et al., 2013] to extend the experimental results. The modeling approach was calibrated to the response of the panel specimens presented in Chapter 3 and validated using data from a database PFRC beam tests developed from the literature presented in Chapter 2. Additional details of the finite element modeling approach and parametric study results can be found in Farag (2024).

4.1. Overview of MCFT and VecTor2

The measured response of the panel specimens from Chapter 3 were used to calibrate a modeling approach using the VecTor2 finite element software [Wong et al. 2013]. VecTor2 utilizes the Modified Compression Field Theory (MCFT) [Vecchio and Collins 1986], which was specifically formulated to simulate cracked reinforced concrete elements subjected to in-plane loads and is the basis for the current shear provisions in the *AASHTO LRFD Bridge Design Specifications* [AASHTO 2020]. Each element consists of cracked concrete and smeared in-plane steel reinforcement and is governed by compatibility and equilibrium equations derived from first principles and constitutive models derived from a series of reinforced concrete panel element tests similar to those performed in this study [Vecchio and Collins 1986].

In recent years, the MCFT has been adapted to FRC by introducing constitutive models to describe the behavior of FRC subjected to uniaxial tension, accounting for the influence of fibers on the tensile behavior of the concrete. In VecTor2 for example, the Variable Engagement Model (VEM) [Voo and Foster, 2003], the Diverse Embedment Model (DEM) [Lee et al., 2011], and the Simplified Diverse Embedment Model (SDEM) [Lee et al., 2013] have all been implemented into the software [Wong et al., 2013].

4.2. Panel Model

Figure 4-1 shows the finite element panel model, which was a single element with a smeared reinforcement representing the longitudinal and transverse bars. This is similar to the panel models developed by others [Carnovale, 2013; Chasioti, 2017; Susetyo, 2009]. The shear was imposed with nodal forces at the corners, which increased with each incremental loading stage.

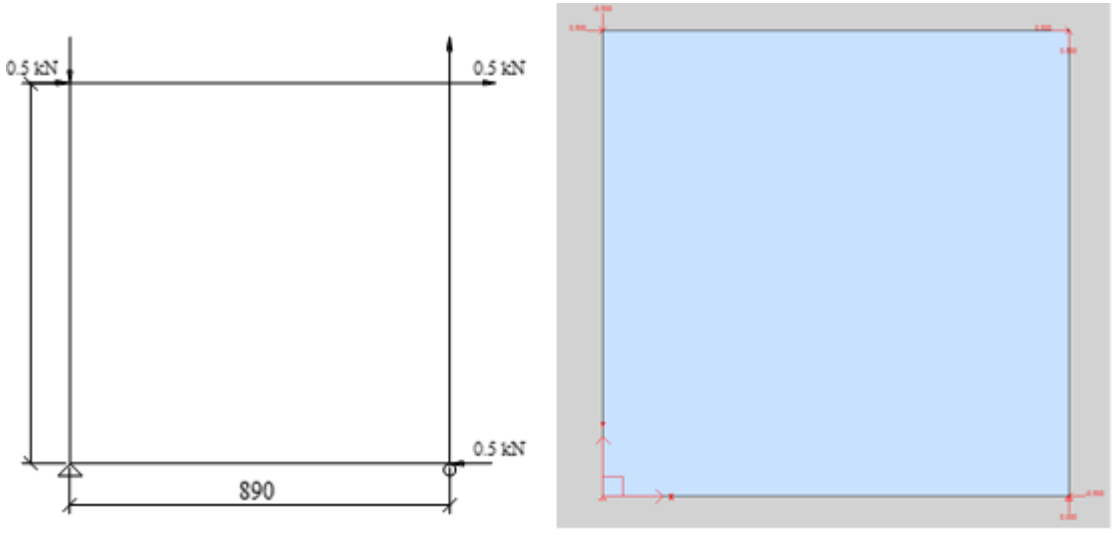

Figure 4-1. VecTor2 model and nodal forces

The constitutive model for the deformed bar reinforcement was calibrated using the results of mechanical tests of five reinforcement samples from the experimental panel elements. For the VT2 model, the constitutive properties for the smeared reinforcement were defined with a yield strength, f_{sy} = 74.3 ksi, an ultimate strength, f_{su} = 101.2 ksi, an elastic modulus, E_s = 26100 ksi. a strain hardening strain, ε_{sh} = 0.013, and an ultimate strain, ε_u =0.18. The measured modulus of the steel was used, rather than a nominal value, to be consistent with the panel element test results. The horizontal reinforcement ratio was fixed at ρ_x = 2.28% for all specimens and ρ_y was specified according to values in Table 3-1, except for the heavily reinforced panels. For these panels, an effective reinforcement ratio of $\rho_{y,e}$ = 0.91% was used instead, neglecting the outermost bars that did not appear to contribute significantly to the measured shear strength, presumably because of their proximity to the toothed anchorage blocks.

The panel models were specified with a thickness of t = 2.75 in with concrete compressive strengths and elastic moduli according to values in Table 3-1. For specimen PFRC-052-000, the elastic modulus was taken as the software default value based on the concrete compressive strength, since modulus data was not available for this specimen. The maximum crack spacing was specified to be equal in x and y direction, $s_x = s_y$ = 2.75 in since the maximum crack spacing did not appear to decrease with fiber content.

4.3. Modeling Approach

Table 4-1 summarizes the constitutive models used in the finite element analyses

Table 4-1. Concrete, reinforcement, and bond constitutive models used in the analyses

Property	Constitutive Model
Concrete	
Compression pre-peak	Hognestad (Parabola)
Compression post-peak	Modified Park-Kent
Compression softening	Vecchio (1992)
Tensions stiffening	Modified Bentz (2005)
Tension softening	Custom input (strain based)
FRC tension	Not used, considered in custom tension softening model
Confined strength	Kupfer / Richart
Dilation	Variable - Isotropic
Cracking criterion	Mohr-Coulomb (Stress)
Crack stress calculation	Basic (DSFM / MCFT)
Crack width check	Agg/2.5 Max Crack Width
Crack slip	Not considered
Creep and relaxation	Not considered
Hysteretic response	Nonlinear w/ plastic offsets
Steel	
Hysteretic response	Bauschinger effect (Seckin)
Dowel action	Tassios (Crack Slip)
Buckling	Akkaya (2012)
Concrete bond	Eligehausen

4.4. Tension Softening Model

The influence of macro-synthetic fibers on the tension behavior of the concrete was integrated into the VecTor2 models using a custom tension softening curve, defined by four points in tension stress-strain space. This approach was necessary because it was found that the existing fiber models integrated into VecTor2 resulted in a post-cracking strength reduction for PFRC, inconsistent with the experimental research findings. The estimated principal tension responses from the panels were used to calibrate a modified exponential tension softening model for macro-synthetic fiber-reinforced concrete that could capture the residual tensile strength observed in the tests,

$$\frac{f_{c1}}{f_{cr}} = (1 - b)e^{-a\,\varepsilon_{c1}} + b \tag{4-1}$$

where ε_{c1} and f_{c1} are the principal tensile strain and stress, f_{cr} is the cracking stress taken as maximum principal tensile stress measured during each of the panel tests, a is a decay parameter, and b defines the residual tensile strength. The constants a and b depend on many factors including concrete mixture design, fiber volume fraction, fiber type, fiber orientation, fiber modulus, among many others. Because the tests presented in Chapter 3 only included a single fiber type and concrete mixture, only fiber volume fraction was considered in the fitting.

Figure 4-2 compares the calibrated tension softening model with the experimental principal tension stress-strain curves. Satisfactory agreement with the measured principal tension curves was found if,

$$a = 450 - 20000\,V_f \geq 50 \tag{4-2}$$

$$b = 3\sqrt{V_f} \tag{4-3}$$

where V_f is the fiber volume fraction (0, 0.0026 and 0.0052 for the tested panels). This clear oversimplification of the phenomena was used to extend the experimental results and further research would be necessary to develop a general curve which accounts for the complex mechanisms of fiber activation and pullout for the various macro-synthetic fibers presently available.

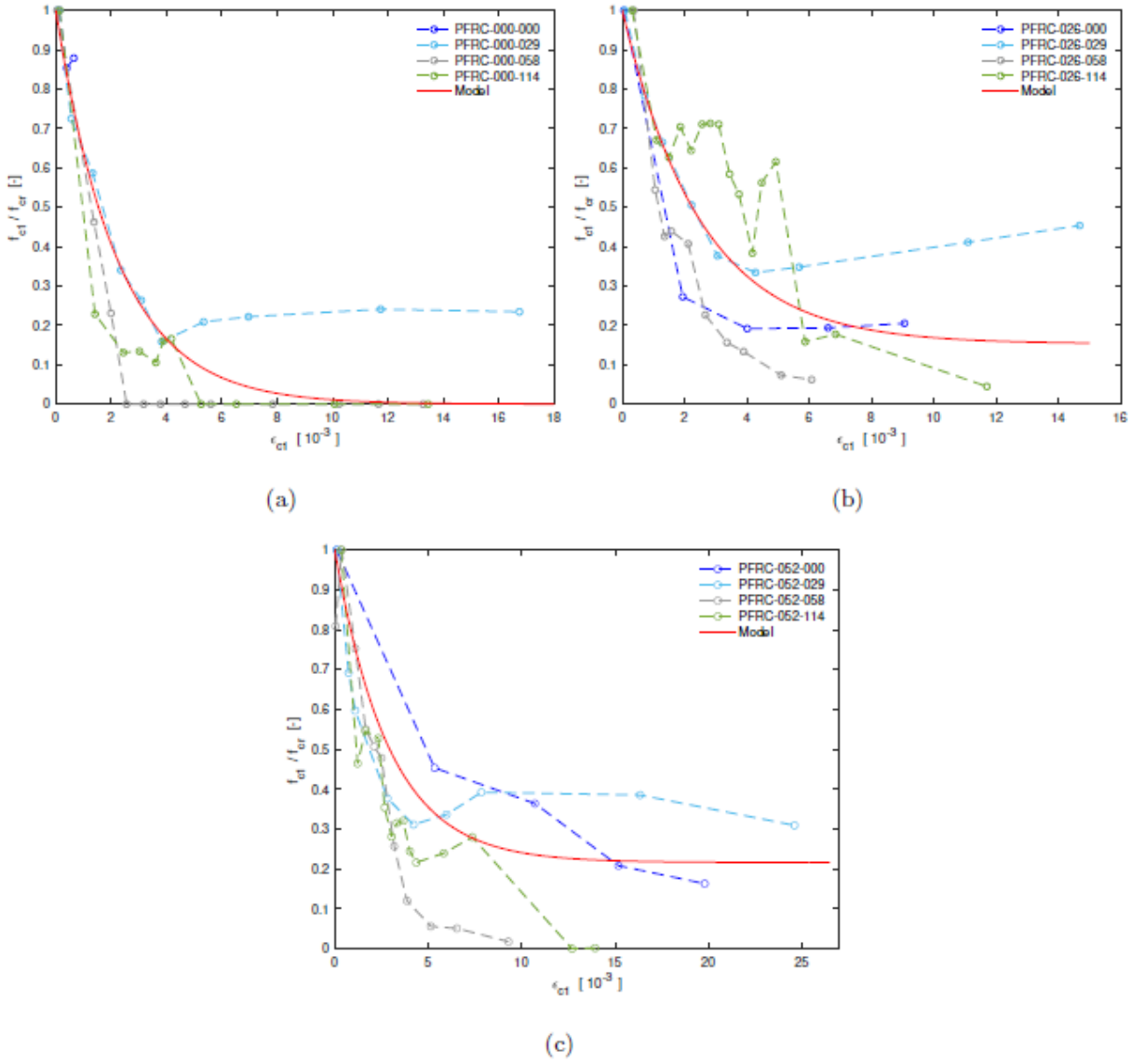

Figure 4-2. Tension softening model (a) Vf = 0% (b) Vf = 0.26%, and (c) Vf = 0.52%

4.5. Panel Model Calibration

Table 4-2 summarizes the calibration results as a ratio of the predicted and experimental shear strengths. Overall, the calibrated models captured the experimental strengths well, the average predicted versus strength ratio was 1.05 with a COV of 11%. As anticipated, the models predicted higher strengths for the two experimental specimens that had consolidation issues during construction (PFRC-026-058 and PFRC-085-058). Without considering these two outliers, the average predicted versus experimental strength ratio was 1.0.

Table 4-2. Experimental and numerical shear strength comparison

Specimen name	v_{exp} (ksi)	v_{vt2} (ksi)	pred/exp
PFRC-000-000	0.31	0.32	1.03
PFRC-000-029	0.62	0.59	0.95
PFRC-000-058	0.78	0.79	1.01
PFRC-000-114	1.13	1.08	0.95
PFRC-026-000	0.20	0.19	0.93
PFRC-026-029	0.63	0.61	0.98
PFRC-026-058	0.61	0.83	1.34
PFRC-026-114	1.08	1.12	1.04
PFRC-052-000	0.22	0.25	1.14
PFRC-052-029	0.73	0.72	0.99
PFRC-052-058	0.72	0.85	1.18
PFRC-052-114	1.08	1.13	1.04

Figure 4-3 shows the numerical and experimental response for a representative panel element with fibers (PFRC-026-029). The models captured important aspects of the panel shear stress-strain behavior, as well as the principal concrete stress-strain response and the progression of the principal stress and strain angles.

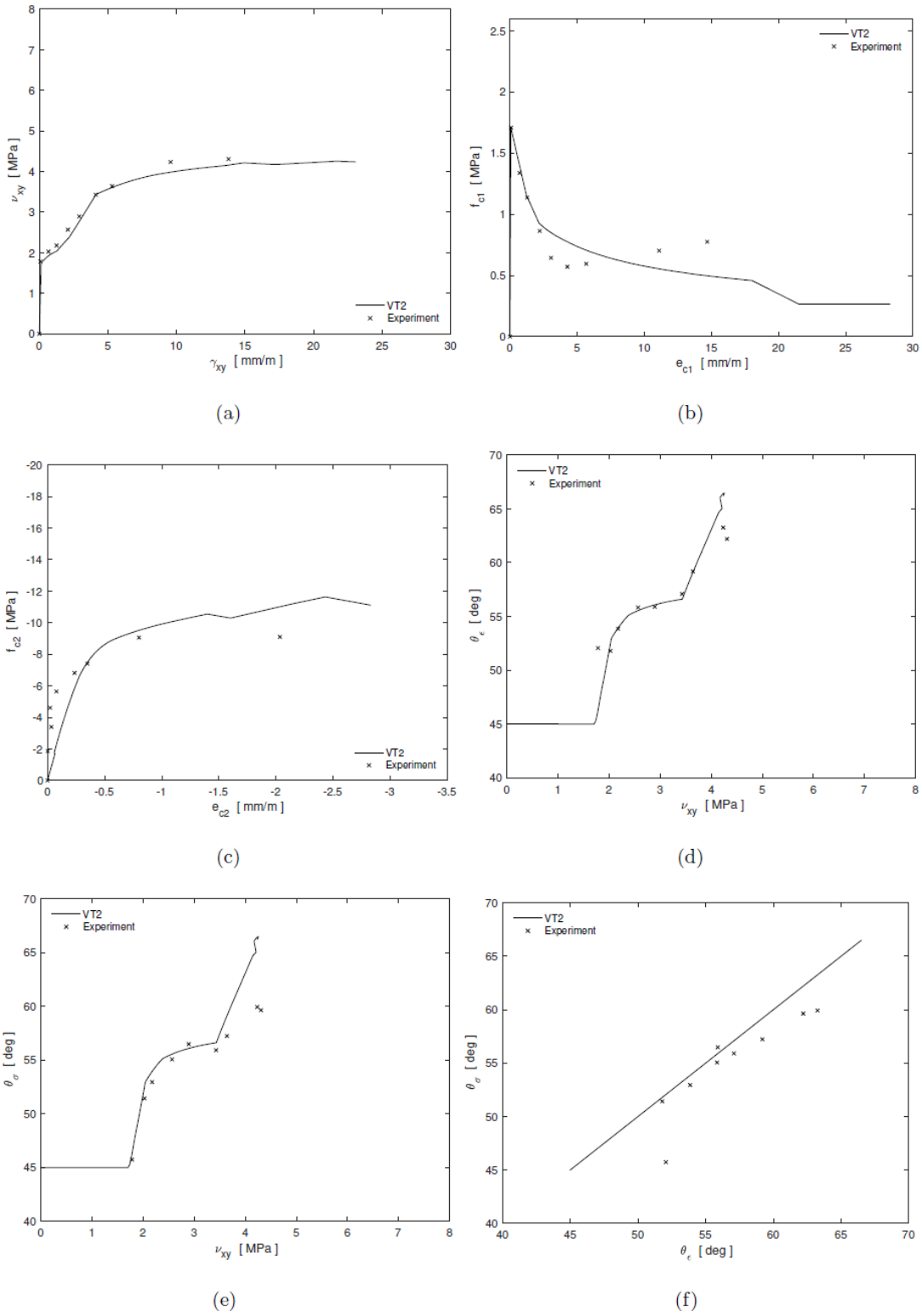

Figure 4-3. Experimental and numerical response for PFRC-026-029 (a) shear stress-strain response (b) concrete principal tension stress-strain, (c) concrete principal compression stress-strain (d) principal strain angle (e) principal stress angle (f) principal stress angle versus principal strain angle (Note: 1 MPa = 0.145 ksi)

4.6. PFRC Modeling Approach Validation

Prior to the experimental program outlined in Chapter 3, only two other PFRC panel tests had been conducted. Carnovale (2013) tested specimens DC-P3 and DC-P5 to investigate if macro-synthetic fibers could replace deformed bar shear reinforcement and compare their performance to panels containing steel fibers. Both specimens incorporated a volume fraction of V_f = 2.0% and were subjected to either monotonic or reverse cyclic loading.

Figure 4-4 compares the shear stress-strain responses of the experimental specimens and finite element models for DC-P3 and DC-P5 tested by Carnovale (2013). The panel specimens were modeled using the approach outlined above with the tensile strength of the concrete taken as the VT2 default tensile strength (blue curve, based on the compressive strength of the concrete) with the softening curve computed using Equation 4-1. The results show that the panel modeling approach can capture the experimental strength within roughly 10% when the default tensile strength is used. However, for panel DC-P5 subjected to reverse cyclic loading, the model over-predicted the strength by approximately 30%, indicating a potential limitation of the proposed tension softening model, which was developed for monotonically loaded specimens.

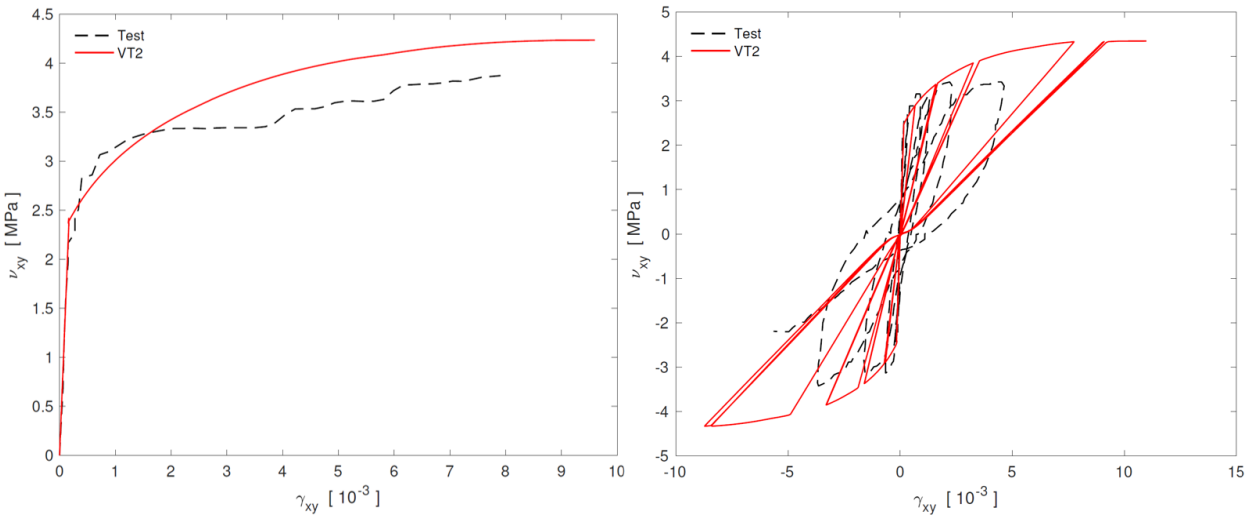

Figure 4-4. Predicted versus experimental results for panels DC-P3 and DC-P5, tested by Carnovale (2013) (Note: 1 MPa = 0.145 ksi)

A larger number of PFRC beams have been tested in flexure, although the available literature is still quite limited. Experimental programs have investigated various fiber types, differing in both geometry and mechanical properties. A total of nine experimental programs were identified, and the specimen geometry and load-displacement response were collected into a database. The beam database included 72 beams total, including 37 PFRC beams without stirrups, 11 PFRC beams with stirrups, 15 RC "control" beams without fibers, and 9 RC beams without fibers with stirrups. The database included beams with span-to-depth ratios ranging from 1.7 to 5.2, concrete compressive strengths from 2.0 ksi to 6.8 ksi, transverse reinforcement ratios from 0% to 3%, and fiber volume fractions from 0% to 3%.

Table 4-3 summarizes the specimens in the beam database and the results of the validation study. The peak measured shear stress during the experiments is reported as well as the predicted shear strength using the finite element models.

Figure 4-5 shows the typical model geometry used for the validation studies. Due to symmetry, only one half of the beams were modeled, with a horizontal roller at the support and appropriate symmetry conditions at the center. The element size was chosen such that at least 10 elements would span the height of the specimen, and the elements were roughly square. The longitudinal reinforcement was modeled explicitly, while transverse reinforcement was included as smeared reinforcement within the elements.

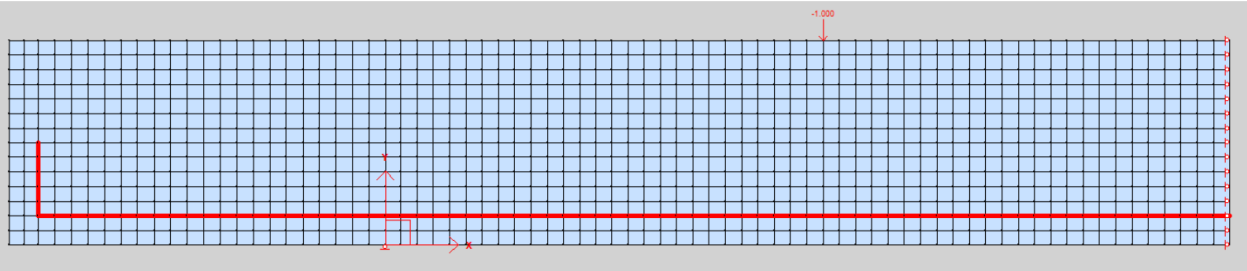

Figure 4-5. VecTor2 model geometry for W430PC, tested by Conforti et al. (2015)

Whenever experimental values of elastic modulus and aggregate size were available, they were specified for the concrete material. The default values in the software, based on the compressive strength of the concrete, were assigned for all the other concrete material properties, except for the crack spacing. The crack spacing was determined according to the guidance in the AASHTO LRFD SBD (AASHTO 2012), where $s_{xe} = s_x \cdot 1.38/(a_g + 0.63)$ is the crack spacing parameter as influenced by aggregate size (12.0 in $\leq s_{xe} \leq$ 80.0 in), a_g is the maximum aggregate size for the concrete in inches, and the crack spacing, s_x, is taken as the effective member depth, d_v, or the maximum distance between layers of longitudinal crack control reinforcement, whichever is less. An upper limit on the crack spacing equal to the member depth h was also imposed, similar to Zhang (2020). For beams with transverse deformed bar reinforcement, the crack spacing was further limited to the stirrup spacing, *s*. The elastic modulus of the steel reinforcement was taken as E_s = 29 000 ksi for all specimens. The yield and ultimate stress were taken as the experimental values if reported, or the assumed yield and ultimate stress, f_{sy} = 60 ksi and f_{su} = 90 ksi, corresponding to Grade 60 rebar.

Figure 4-6 compares the experimental and numerical load-deformation response for two representative beam specimens. Given the wide range of aspect ratios, reinforcement ratios, fiber volumes, and concrete compressive strengths contained within the database, if was concluded that satisfactory prediction of the peak strength was achieved (see Table 4-3), while other aspects of the force-deformation response were not.

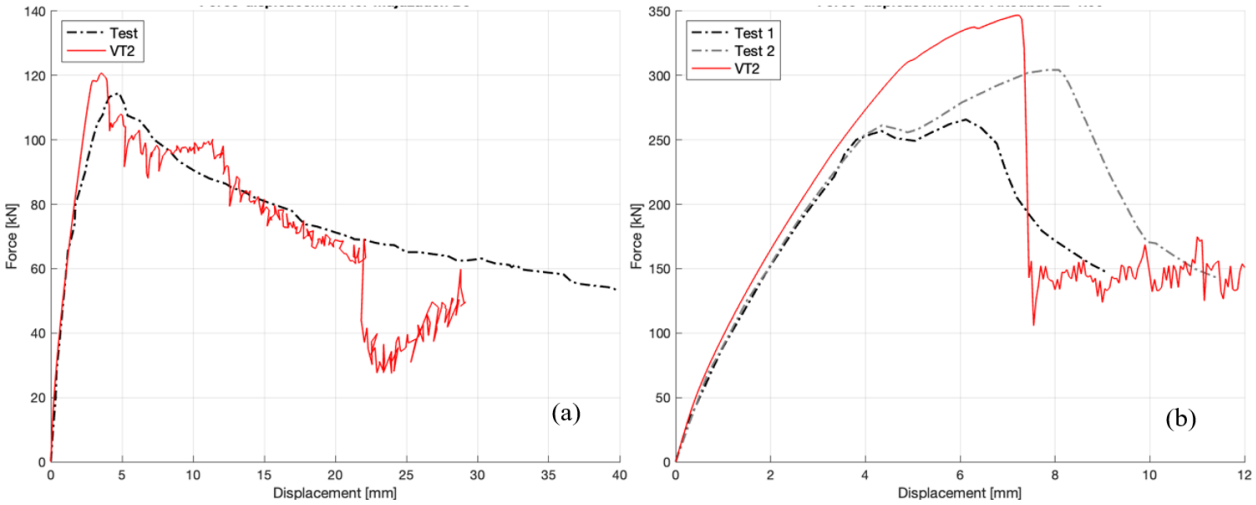

Figure 4-6. Load-deformation response of representative PFRC beam specimens (a) B3 from Majdzadeh et al. 2006 (b) L2-1.00 from Altoubat et al. 2009 (Note: 1 kN = 0.225 kip, 1 mm = 0.039 in)

Figure 4-7 shows the numerical shear strengths plotted against the experimental shear strengths for the specimens in the PFRC beam database. The shear capacity of the beams in Table 4-3 spans from 0.15 ksi to 0.6 ksi. The modeling approach predicted the shear strength of the full range with reasonable accuracy. The shear strength of the beams tested by Murad & Abdel-Jabbar (2022) and the lower aspect ratio beams tested by Altoubat et al. (2009) were notably overpredicted (numerical-to-experimental shear strength ratios > 1.5). These beams had span-to-depth ratios, $a/d \leq 2.3$, putting them in the lowest quartile of the experimental database in terms of span length, which may have contributed to the overprediction. Overall, the average predicted to experimental strength ratio for the beams in Table 4-3 was 1.13 with a COV of 24%.

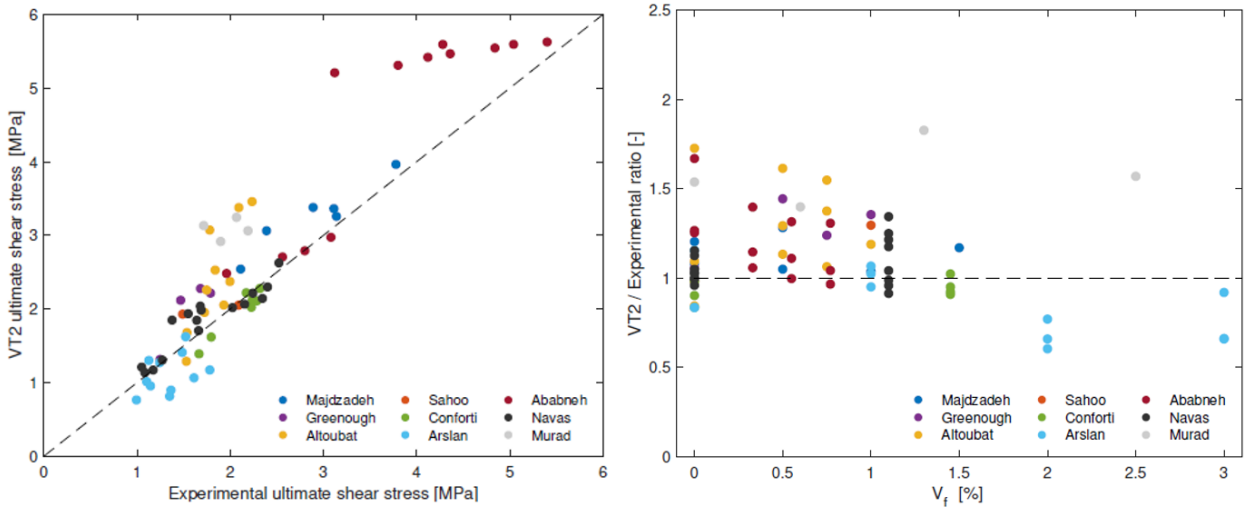

Figure 4-7. Numerical versus experimental shear strength for the PFRC beam database (Note: 1 MPa = 0.145 ksi)

Table 4-3. Database of PFRC beams tested in flexure

Reference	Specimen ID	d (in)	a/d	ρ_l (%)	ρ_t (%)	f_c (ksi)	V_f (%)	l_f (in)	AR	$v_{u,exp}$ (ksi)	$v_{u,pred}$ (ksi)	pred/exp
Majdzadeh et al. (2006)	B1	4.7	3	2.62	0.28	6.6	-	-	-	0.45	0.49	1.09
	B2	4.7	3	2.62	-	6.8	-	-	-	0.31	0.36	1.18
	B3	4.7	3	2.62	0.28	5.5	0.5	2.0	85	0.55	0.48	0.88
	B6	4.7	3	2.62	-	6.4	0.5	2.0	85	0.35	0.44	1.28
	B7	4.7	3	2.62	-	6.4	1	2.0	85	0.46	0.47	1.04
	B8	4.7	3	2.62	-	6.3	1.5	2.0	85	0.42	0.49	1.17
Greenough & Nehdi (2008)	Reference	10.4	3	1.78	-	5.7	-	-	-	0.18	0.19	1.05
	P-WV-50-0.5	10.4	3	1.78	-	6.1	0.5	2.0	63	0.21	0.31	1.47
	P-WV-50-0.75	10.4	3	1.78	-	5.7	0.75	2.0	63	0.26	0.32	1.24
	P-WV-50-1.0	10.4	3	1.78	-	5.5	1	2.0	63	0.24	0.33	1.35
Altoubat et al. (2009)	L1-0.0	15.7	3.5	2.15	-	5.9	-	-	-	0.22	0.19	0.85
	L1-0.50	15.7	3.5	2.15	-	6.1	0.5	1.6	90	0.25	0.27	1.1
	L1-0.75	15.7	3.5	2.15	-	6.1	0.75	1.6	90	0.28	0.29	1.04
	L2-0.0	13.0	3.5	3.18	-	5.9	-	-	-	0.22	0.24	1.07
	L2-0.50	13.0	3.5	3.18	-	6.1	0.5	1.6	90	0.25	0.33	1.3
	L2-0.75	13.0	3.5	3.18	-	6.1	0.75	1.6	90	0.27	0.34	1.29
	L2-1.0	13.0	3.5	3.18	-	5.2	1	1.6	90	0.29	0.32	1.12
	Sh2-0.0	13.0	2.3	3.18	-	5.9	-	-	-	0.26	0.43	1.68
	Sh2-0.50	13.0	2.3	3.18	-	6.1	0.5	1.6	90	0.30	0.49	1.61
	Sh2-0.75	13.0	2.3	3.18	-	6.1	0.75	1.6	90	0.32	0.50	1.55
Sahoo et al. (2015)	RC	6.8	5.2	2.34	0.22	5.3	-	-	-	0.30	0.30	0.98
	PFRC	6.8	5.2	2.34	-	5.5	1	0.5	25	0.22	0.28	1.3
Conforti et al. (2015)	W430PC	8.5	2.5	1.3	-	4.5	-	-	-	0.26	0.23	0.9
	W510PFRC	10.0	2.5	1.24	-	3.8	1.45	1.6	53	0.32	0.31	0.95
	W650PFRC	8.5	3	1.15	-	3.8	1.45	1.6	53	0.31	0.32	1.02
	W770PC	10.0	2.5	1.23	-	4.5	-	-	-	0.24	0.20	0.83

Reference	Specimen ID	d (in)	a/d	ρ_l (%)	ρ_t (%)	f_c (ksi)	V_f (%)	l_f (in)	AR	$v_{u,exp}$ (ksi)	$v_{u,pred}$ (ksi)	pred/exp
	W770MSR	10.0	2.5	1.23	0.1	4.5	-	-	-	0.34	0.33	0.98
	W770PFRC	10.0	2.5	1.23	-	3.8	1.45	1.6	53	0.33	0.31	0.92
	W890PFRC	11.6	2.2	1.23	-	3.8	1.45	1.6	53	0.32	0.29	0.91
Arslan et al. (2017)	B2.5R	8.3	2.5	1.28	-	3.8	-	-	-	0.16	0.19	1.15
	2.5P1.0	8.3	2.5	1.28	-	3.9	1	1.5	51	0.22	0.23	1.06
	2.5P2.0	8.3	2.5	1.28	-	2.0	2	1.5	51	0.20	0.13	0.66
	2.5P3.0	8.3	2.5	1.28	-	2.7	3	1.5	51	0.26	0.17	0.66
	B3.5R	8.3	3.5	1.28	-	3.8	-	-	-	0.17	0.14	0.83
	B3.5P1.0	8.3	3.5	1.28	-	3.9	1	1.5	51	0.21	0.21	0.95
	B3.5P2.0	8.3	3.5	1.28	-	2.0	2	1.5	51	0.20	0.12	0.6
	B3.5P3.0	8.3	3.5	1.28	-	2.7	3	1.5	51	0.23	0.15	0.66
	4.5P1.0	8.3	4.5	1.28	-	3.9	1	1.5	51	0.18	0.18	1.02
	B4.5P2.0	8.3	4.5	1.28	-	2.0	2	1.5	51	0.14	0.11	0.76
	B4.5P3.0	8.3	4.5	1.28	-	2.7	3	1.5	51	0.16	0.15	0.92
Ababneh et al. (2017)	B1V0S0	4.9	2.4	3.22	-	6.3	-	-	-	0.28	0.36	1.26
	B1V3S0	4.9	2.4	3.22	-	6.4	0.33	1.6	90	0.37	0.39	1.05
	B1V5S0	4.9	2.4	3.22	-	6.5	0.55	1.6	90	0.41	0.41	1.01
	B1V7S0	4.9	2.4	3.22	-	6.7	0.77	1.6	90	0.45	0.43	0.97
	B2V0S30	4.9	2.4	3.22	3.35	6.3	-	-	-	0.63	0.79	1.26
	B2V3S30	4.9	2.4	3.22	3.35	6.4	0.33	1.6	90	0.70	0.81	1.15
	B2V5S30	4.9	2.4	3.22	3.35	6.5	0.55	1.6	90	0.73	0.81	1.11
	B2V7S30	4.9	2.4	3.22	3.35	6.7	0.77	1.6	90	0.78	0.81	1.04
	B3V0S60	4.9	2.4	3.22	1.68	6.3	-	-	-	0.45	0.76	1.67
	B3V3S60	4.9	2.4	3.22	1.68	6.4	0.33	1.6	90	0.55	1.19	2.16
	B3V5S60	4.9	2.4	3.22	1.68	6.5	0.55	1.6	90	0.60	0.79	1.32
	B3V7S60	4.9	2.4	3.22	1.68	6.7	0.77	1.6	90	0.62	0.82	1.31
Navas et al. (2018)	OA1	18.6	3.9	1.68	-	6.1	-	-	-	0.16	0.17	1.05
	OA2	18.7	4.8	2.23	-	6.1	-	-	-	0.17	0.17	1

Reference	Specimen ID	d (in)	a/d	ρ_l (%)	ρ_t (%)	f_c (ksi)	V_f (%)	l_f (in)	AR	$v_{u,exp}$ (ksi)	$v_{u,pred}$ (ksi)	pred/exp
	OB1	18.6	3.9	2.23	-	5.6	-	-	-	0.18	0.18	0.99
	OB2	18.5	4.8	2.24	-	5.8	-	-	-	0.15	0.17	1.11
	A1	18.6	3.9	1.68	0.1	5.8	-	-	-	0.24	0.27	1.12
	A2	18.6	4.8	2.23	0.1	5.9	-	-	-	0.24	0.25	1.03
	B1	18.7	3.9	2.22	0.15	5.8	-	-	-	0.31	0.30	0.95
	B2	18.7	4.8	2.22	0.15	5.9	-	-	-	0.29	0.29	1
	OAP1	18.6	3.9	1.67	-	6.3	1.1	1.9	56	0.22	0.28	1.25
	OAP2	18.6	4.8	2.23	-	6.5	1.1	1.9	56	0.25	0.29	1.18
	OBP1	18.5	3.9	2.24	-	6.2	1.1	1.9	56	0.24	0.29	1.21
	OBP2	18.5	4.9	2.25	-	6.1	1.1	1.9	56	0.20	0.27	1.34
	AP1	18.7	3.9	1.67	0.1	6.4	1.1	1.9	56	0.35	0.33	0.96
	AP2	18.7	4.8	2.23	0.1	6.5	1.1	1.9	56	0.34	0.31	0.91
	BP1	18.9	3.8	2.19	0.15	6.5	1.1	1.9	56	0.37	0.38	1.04
	BP2	18.7	4.8	2.22	0.15	6.4	1.1	1.9	56	0.32	0.32	0.98
Murad & Abdel-Jabbar (2022)	Control	8.9	1.7	1.19	-	6.0	-	-	-	0.28	0.39	1.43
	P2	8.9	1.7	1.19	-	6.6	0.6	2.1	68	0.32	0.44	1.39
	P4	8.9	1.7	1.19	-	5.9	1.3	2.1	68	0.25	0.45	1.82
	P8	8.9	1.7	1.19	-	5.5	2.5	2.1	68	0.30	0.47	1.56

4.7. Parametric Study

The objective of the parametric study was to extend the results of the experimental testing program, exploring additional combinations of parameters that were not, or could not be, tested experimentally. For example, the experimental panels had a maximum fiber content of 0.52% by volume, which was done to prevent consolidation issues with higher fiber content as has been seen by others [e.g., Sahoo et al. 2015 and Lee et al. 2019]. Utilizing the fitted tension softening model parameters and Equation 4-1, it was possible to estimate the strength provided by fiber contents up to 2.0%, which was the largest fiber volume fraction in the panel tests that were used for calibration and validation of the modeling approach.

In addition to the fiber volume, $0\% \leq V_f \leq 2.0\%$, the other parameters of interest were the transverse reinforcement ratio, $0\% \leq \rho_y \leq 1.5\%$, and the concrete's compressive strength, 2.9 ksi $\leq f_c \leq$ 13.8 ksi. Exploring a range of combinations of ρ_y, V_f, and f_c was intended to give an understanding about regions of the design space where the addition of macro-synthetic fibers would be most beneficial. In total, 288 combinations of parameters were identified and panel element models with each combination were built using the modeling approach outlined above. A fixed maximum crack spacing of 2.75 in was used for all panel models to be consistent with the experimental results presented in Chapter 3; the response of the panels was not found to be highly sensitive to the selection of this parameter. The analyses focused on shear strength and deformation capacity (shear strain at failure).

Figure 4-8 shows typical shear stress-strain responses for panel models in the parametric study. Generally, shear strength increased with a higher transverse reinforcement ratio and fiber volume fraction, while the shear strain at failure decreased. The addition of volume fractions of fibers, $V_f \leq 0.5\%$, led to minimal improvements to the shear strength; the shear stress-strain response of the panels in Figure 4-8c with fiber volume fractions, $V_f = 0\%$, 0.25% and 0.5%, were indistinguishable after a shear strain of 0.004. The exception to these trends were the panels without transverse reinforcement, where the addition of fibers, at any volume fraction, was seen to increase the shear strength and shear strain at failure.

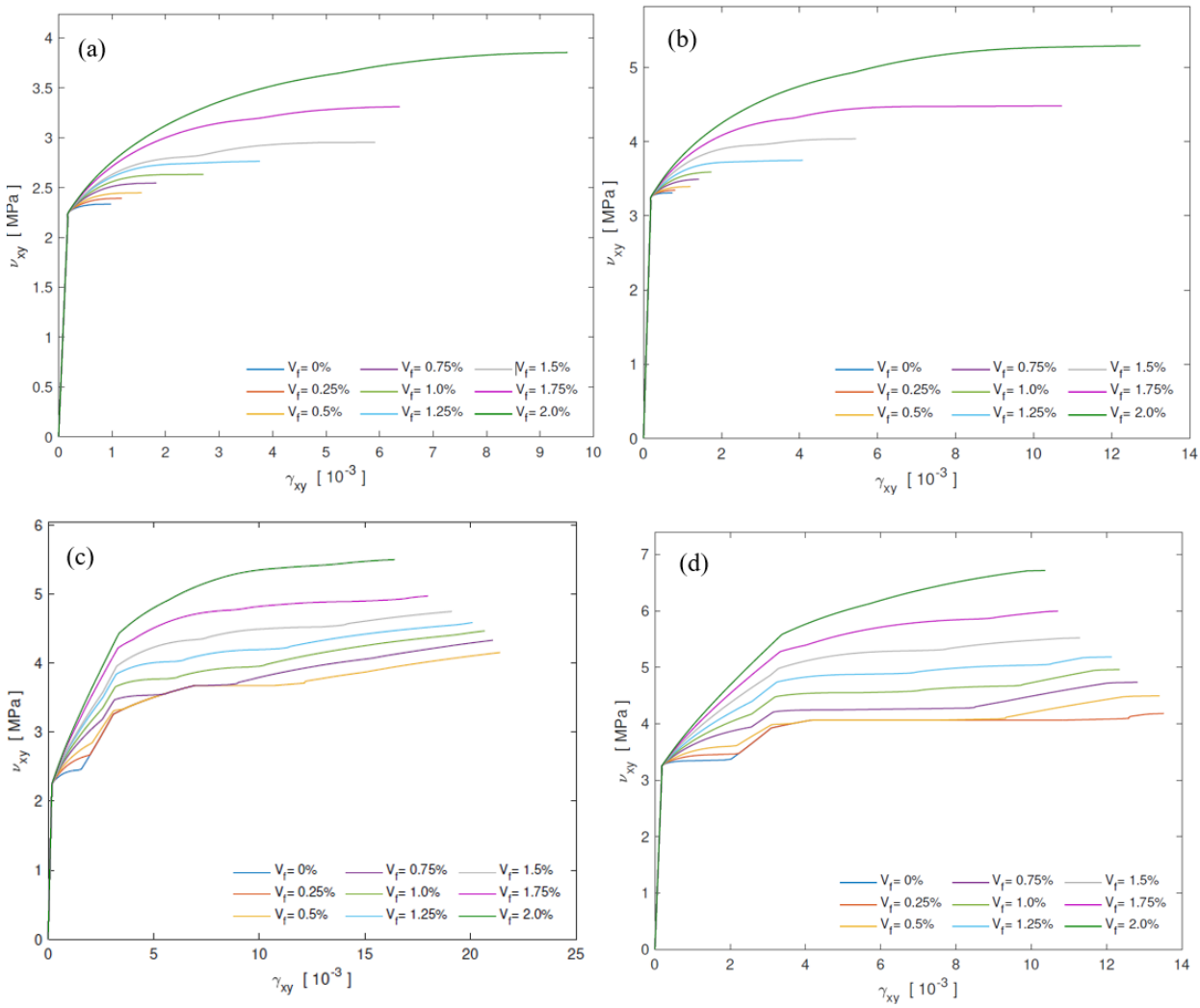

Figure 4-8. Shear stress-strain responses for panel models in the parametric study for the range of fiber volume fractions considered (a) ρ_y =0.00% and f'_c =6.5 ksi, (b) ρ_y =0.00% and f'_c =13.8 ksi (c) ρ_y =0.25% and f'_c =6.5 ksi, (d) ρ_y =0.25% and f'_c =13.8 ksi

Figure 4-9 shows the shear strength improvement realized for different fiber addition rates for the transverse reinforcement ratios and concrete strengths considered in the parametric study. The shear strength improvement was calculated by dividing the shear strength of the model by the shear strength of the corresponding model without fibers (but with the same concrete compressive strength and transverse reinforcement ratio). The strength improvement from the addition of macro-synthetic fibers was found to be greater (as a percentage) for panels with $f_c \geq$ 10 ksi compared to the panels with $f_c \leq 6$ ksi and was less pronounced for panels with high transverse reinforcement ratios ($\rho_y > 0.75\%$) than less reinforced counterparts ($\rho_y \leq 0.5\%$). In the range of the parameters investigated experimentally, $V_f \leq 0.52\%$, strength improvement was typically less than 10%, which given experimental uncertainties, may explain why no discernable strength decrease (or increase) was seen in the experimental panel test series. Interestingly, the greatest improvements in shear strength (as a percentage) from macro-synthetic fiber addition were for panels that were lightly reinforced (ρ_y = 0.1% and ρ_y = 0.25%), more than those panels

that did not contain transverse reinforcement (ρ_y = 0%). Furthermore, the effectiveness of fibers generally decreased with a greater amount of transverse reinforcement, regardless of concrete strength.

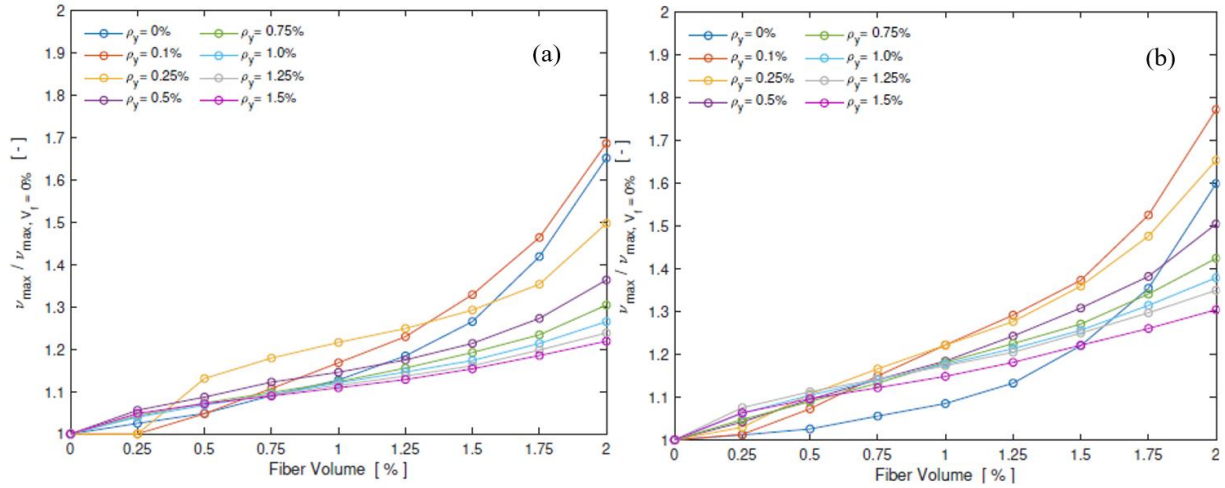

Figure 4-9. Shear strength improvement for different fiber addition rates for the transverse reinforcement ratios considered in the parametric study (a) f'_c =6.5 ksi and (b) f'_c =13.8 ksi

Figure 4-10 shows the contour plot of the shear strength (in MPa, 1 MPa = 0.145 ksi) of the models as a function of the transverse reinforcement ratio, ρ_y, and fiber volume fraction, V_f, for panels with f'_c = 6.5 ksi. The plots for other concrete strengths are similar in shape, but different in magnitude. Evident from the figure, panel shear strength increases with increases in either variable, albeit at different rates. There also appears to be some interaction between the volume fiber fraction and reinforcement ratio, although the effect on the contours is minimal. For a given target shear strength, for example 0.725 ksi (≈ 5 MPa), the addition of macro-synthetic fibers on the order of Vf = 1.5% by volume was seen to reduce the amount of required transverse deformed bar reinforcement by roughly half.

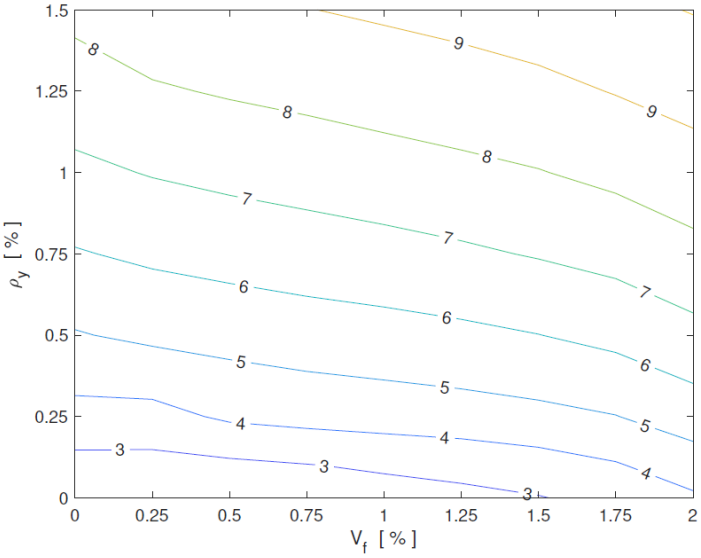

Figure 4-10. Shear strength contour plot for f'_c = 6.5 ksi

Figure 4-11 shows the maximum crack width at a normalized shear stress of $0.13\sqrt{f'c}$ (ksi) plotted against transverse reinforcement ratio and fiber volume fraction. The panels without transverse reinforcement and some of the panels with ρ_y=0.125% did not reach this shear stress level and are, therefore, not shown in the plot. Similar to the experimentally tested panels, the maximum crack width at a normalized shear stress of $0.13\sqrt{f'c}$ (ksi) tended to decrease as either the transverse reinforcement ratio or fiber volume increased. Also, the effectiveness of macro-synthetic fibers to arrest crack widths decreased as the transverse reinforcement ratio increased and vice versa.

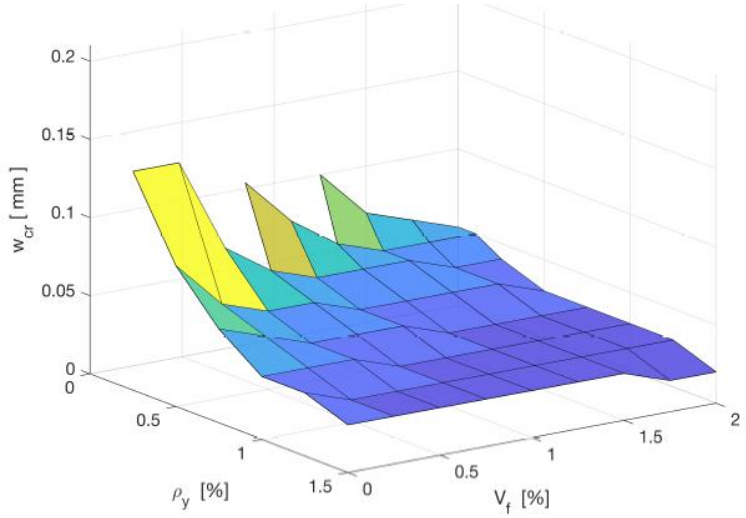

Figure 4-11. Maximum crack width at a normalized shear stress of $0.13\sqrt{f'c}$ (ksi) for f'_c =6.5 ksi

CHAPTER 5. COMPARISON WITH EMPIRICAL SHEAR STRENGTH EQUATIONS

The shear strengths of the PFRC beam database developed from the literature presented in Chapter 2, the experimentally tested PFRC panels presented in Chapter 3, and the finite element panel models presented in Chapter 4 were compared to shear strength prediction equations specified in several model codes.

5.1. Shear Strength Prediction Equations

These codes were selected because they handle the shear strength of concrete members and presence of fibers differently:

- The *AASHTO LRFD Bridge Design Specifications* [AASHTO 2020] uses the MCFT to estimate the shear strengths of structural elements and does not address fiber's contribution to the shear strength of members;
- The *ACI 318* [ACI 2019] permits the use of SFRC beams without stirrups if certain criteria are met, however the shear strength of FRC is conservatively assumed equal to that of conventional concrete; and
- The *fib Model Code 2010* [*fib* 2013] contains shear strength expression for FRC that includes the post cracking strength of the concrete as a design parameter, f_{Ftuk}, which is influenced by the presence and volume fraction of fibers.

5.1.1. AASHTO LRFD Bridge Design Specifications

The basis for the current shear provisions in the *AASHTO LRFD Bridge Design Specifications* [AASHTO 2020] is the Modified Compression Field Theory (MCFT) [Vecchio and Collins 1986]. According to the MCFT, the shear strength of a concrete member can be estimated if two parameters, β and θ, are known. These two factors depend on the longitudinal strain in the element and the crack spacing, and values for β and θ can be computed directly or estimated using values in tables for members with and without transverse reinforcement (Bentz et al., 2006). The *AASHTO LRFD Bridge Design Specifications* do not consider the contribution of fibers to a member's shear strength, rather the nominal shear resistance is determined as the sum of contributions from the concrete, transverse steel, and prestressing:

$$v_n = \min \begin{cases} v_c + v_s + v_p \\ 0.25 f'_c + v_p \end{cases} \tag{5-1}$$

$$v_c = 0.0316\beta \cdot \sqrt{f'_c} \tag{5-2}$$

$$v_s = \frac{A_v f_y \cdot (\cot\theta + \cot\alpha)\sin\alpha}{b_v \cdot s} \tag{5-3}$$

where A_v is the area of transverse reinforcement within a distance s, f'_c is the specified concrete cylinder compressive strength in ksi, f_y is the yield stress of the transverse reinforcement in ksi, b_v is the effective web width, β is a parameter that accounts for the concrete's ability to transmit tensile stresses, θ is the angle of inclination of compressive stress, and α is the angle of inclination of transverse reinforcement. The parameters β and θ are calculated as:

$$\beta = \frac{4.8}{1+750\epsilon_x} \text{ for } A_v \geq 0.083\sqrt{f'_c} \cdot \frac{b_v \cdot s}{f_y} \tag{5-4}$$

$$\beta = \frac{4.8}{1+750\epsilon_x} \cdot \frac{51}{39+s_{xe}} \text{for } A_v < 0.083\sqrt{f'_c} \cdot \frac{b_v \cdot s}{f_y} \quad (5\text{-}5)$$

$$\theta = 29 + 3500\epsilon_x \quad (5\text{-}6)$$

Where $s_{xe} = s_x \cdot 1.38/(a_g + 0.63)$ is the crack spacing parameter as influenced by aggregate size (12.0 in $\leq s_{xe} \leq$ 80.0 in), a_g is the maximum aggregate size for the concrete in inches, and the crack spacing, s_x, is taken as the effective member depth, d_v, or the maximum distance between layers of longitudinal crack control reinforcement, whichever is less. The net longitudinal strain in the section at the centroid of the tensile reinforcement, ϵ_x, is computed as:

$$\epsilon_x = \frac{\frac{|M_u|}{d_v} + 0.5N_u + 0.5|V_u - V_p| - A_{ps}f_{po}}{E_s A_s + E_p A_{ps}} \quad (5\text{-}7)$$

where M_u is the factored moment at the section, N_u is the factored axial force at the section, V_u is the factored shear force at the section, V_p is the component of prestressing force in the direction of the shear force, f_{po} is the effective prestress in the prestressed reinforcement (often taken as $0.7f_{pu}$), and E_s, A_s, E_p, and A_{ps} are the elastic modulus and area of the non-prestressed and prestressed tension reinforcement on the flexural tension side of the member, respectively.

5.1.2. ACI 318

Although ACI-318 [ACI 2019] permits the use of SFRC beams without stirrups if certain criteria are met, it does not quantify the contribution of fiber-reinforcement to the strength of structural elements; the shear strength of FRC for non-prestressed members is conservatively assumed equal to that of conventional concrete, similar to the *AASHTO LRFD Bridge Design Specifications*.

$$v_c = \left[8\lambda_s\lambda(\rho_w)^{1/3}\sqrt{f'_c} + \frac{N_u}{6A_g}\right] \quad (5\text{-}8)$$

where N_u is the axial force on the cross section, A_g the gross area of the cross section, ρ_w is the longitudinal reinforcement ratio for the web, f'_c is the 28-day cylinder strength in psi, λ is a factor to account for lightweight concrete, and λ_s is the size effect factor, computed as

$$\lambda_s = \begin{cases} 1.0, & \text{if } A_v \geq A_{v,min} \\ \sqrt{\frac{2}{1+0.1\cdot d}} \leq 1.0, & \text{if } A_v < A_{v,min} \end{cases} \quad (5\text{-}9)$$

The minimum transverse reinforcement ratio $A_{v,min}$ is determined by:

$$A_{\text{v,min}} = \max\left(0.75\sqrt{f'_c} \cdot \frac{b_w}{f_{yt}}, \quad 50 \cdot \frac{b_w \cdot s}{f_{yt}}\right) \quad (5\text{-}10)$$

where b_w is the width of the web of the section, s is the transverse reinforcement spacing, and f_{yt} is the yield stress of the transverse reinforcement in psi. The contribution of the transverse reinforcement is computed similarly to the AASHTO and *fib* codes, however ACI 318 assumes an inclination, θ=45°, which simplifies the calculation. ACI 318 imposes an upper limit for the transverse reinforcement strength contribution of $v_s \leq 8\sqrt{f'_c}$ (f'_c in psi).

5.1.3. fib Model Code 2010

The fib Model Code 2010 considers the benefit of fibers to the shear strength of concrete, specifying the shear strength contribution of FRC as:

$$v_{Rd,F} = \frac{0.18}{\gamma_c} k \left[100\rho \left(1 + 7.5 \frac{f_{Ftuk}}{f_{ctk}}\right) f'_c\right]^{1/3} + 0.15\sigma_{cp} \geq 0.035 k^{3/2} \sqrt{f'_c} + 0.15\sigma_{cp} \quad (5\text{-}11)$$

where γ_c is the partial safety factor for concrete (taken as 1.0 for comparison to experimental strengths), σ_{cp} is the compressive stress in the element caused by external loads or prestressing, f'_c is the 28-day compressive cylinder strength in MPa, ρ is the longitudinal reinforcement ratio, $k = 1 + \sqrt{200/d} \leq 2.0$ is a size effect factor that depends on the member depth *d* (in mm), f_{Ftuk} is the characteristic value of the ultimate residual tensile strength, and f_{ctk}.For a crack width at ultimate, w_u=1.5 mm:

$$f_{Ftuk} = f_{Fts} - \frac{w_u}{CMOD_3}(f_{Fts} - 0.5 f_{R3} + 0.2 f_{R1}) \geq 0 \quad (5\text{-}12)$$

where f_{R1} and f_{R3} are the residual strengths from an FRC flexural test at $CMOD_3$=0.5 mm and $CMOD_3$=2.5 mm, respectively. The residual strengths can be estimated by

$$f_{R3} = 6.0 \cdot \left(V_f \cdot \frac{l_f}{d_f}\right)^{0.7} \quad (5\text{-}13)$$

$$f_{R1} = 7.5 \cdot \left(V_f \cdot \frac{l_f}{d_f}\right)^{0.8} \quad (5\text{-}14)$$

$$f_{Fts} = 0.45 f_{R1}. \quad (5\text{-}15)$$

The characteristic tensile strength f_{ctk} is taken as f_{ctm} according to :

$$f_{ctm} = 0.3(f_{ck})^{2/3} \quad \text{for } f'_c \leq 50 \text{ MPa} \quad (5\text{-}16)$$

$$f_{ctm} = 2.12 \cdot \ln\left(1 + 0.1(f'_c + \Delta f)\right) \quad \text{for } f'_c > 50 \text{ MPa} \quad (5\text{-}17)$$

where Δf =8 MPa. If the transverse reinforcement ratio, $\rho_t > 0.08\sqrt{f'_c}/f_y$, the shear resistance of the member is taken as the sum of concrete and transverse steel contributions:

$$v_{Rd} = v_{Rd,F} + v_{Rd,s} \leq v_{Rd,max} \quad (5\text{-}18)$$

The contribution from the transverse reinforcement and the strength limit are computed by:

$$v_{Rd,max} = k_\epsilon \cdot \frac{f'_c}{\gamma_c} \cdot \sin\theta \ \cos\theta \quad (5\text{-}19)$$

$$v_{Rd,s} = \frac{A_s}{s \cdot b_w} \cdot f_y \cot\theta \quad (5\text{-}20)$$

where $\theta_{\min} \leq \theta \leq 45°$, $\theta_{\min} = 20° + 10\,000\epsilon_x$, and

$$k_\epsilon = \frac{1}{1.2 + 55\epsilon_1} \leq 0.65 \quad (5\text{-}21)$$

$$\epsilon_1 = \epsilon_x + (\epsilon_x + 0.002)\cot^2\theta \quad (5\text{-}22)$$

The longitudinal strain, ϵ_x, is determined by:

$$\epsilon_x = \frac{1}{2E_s A_s}\left(\frac{M_{Ed}}{z} + V_{Ed} + N_{Ed}\left(\frac{1}{2} - \frac{\Delta e}{z}\right)\right) \quad (5\text{-}23)$$

where M_{Ed}, V_{Ed}, and N_{Ed} are the design moment, shear, and axial load at the section under consideration; Δe is the distance from the sections geometric centroid to mid-depth of the effective shear depth; z is the effective shear depth that can be assumed equal to $0.9d$; and E_s and A_s are the elastic modulus and area of the non-prestressed tension reinforcement.

5.2. Evaluation of empirical equations

The shear strength prediction equations were evaluated using the shear strengths of the PFRC beam database developed from the literature presented in Chapter 2, the experimentally tested PFRC panels presented in Chapter 3, and the finite element panel models presented in Chapter 4.

Figure 5-1a shows the predicted panel strength from the empirical equations versus the measured shear strength of the tested panels presented in Chapter 3. The dashed line indicates a 1:1 relationship. Fig. 5-1b shows the ratio of the predicted to the measured shear strength for the panels, excluding the two panels that experienced consolidation issues during casting (PFRC-026-058 and PFRC-052-058). The dashed line indicates a predicted-to-measured shear strength ratio of 1.0. An effective reinforcement ratio of 0.91% was used to compute the strengths for the highly reinforced panels, ignoring the transverse deformed bar reinforcement in the highly disturbed region directly adjacent to the anchor blocks, which was found to give more accurate representation of the reinforcement contribution in the finite element calibration in Chapter 4.

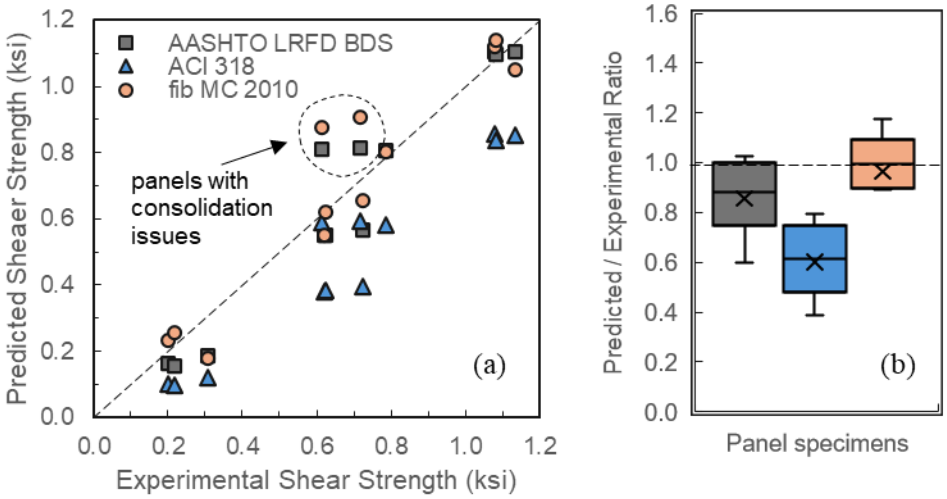

Figure 5-1. Empirical shear strength prediction of tested PFRC panels (a) predicted versus experimental shear strength (b) predicted-to-measured shear strength ratio

In general, the model code equations did a reasonable job of capturing the strength of the tested panels and were conservative, except for the two panels with had consolidation issues during casting. The equations developed by AASHTO and *fib* estimated higher shear strengths than ACI 318, which was the most conservative of the three. The *fib Model Code 2010* was the most accurate with a mean predicted-to-measured shear strength ratio of 0.97 and a COV of 17% and the ACI 318 equation was the least accurate with a mean predicted-to-measured shear strength ratio of 0.62 and a COV of 23%. Given that the ACI 318 equation does not account for the presence of fibers and predicted the shear strength of the panels solely on their concrete compressive strength, the similar COV values between the *fib* Model Code 2010 and ACI 318 equations would support the assertion that the macro-synthetic fibers had a limited contribution

to the shear strength of the panels, at the volume fractions experimentally investigated. The shear strength equations developed by AASHTO had a mean predicted-to-measured shear strength ratio of 0.87 and a COV of 17%.

Figure 5-2 shows the ratio of the predicted to the measured shear strength for the beam specimens from the collected beam database summarized in Table 4-3. The dashed line indicates a predicted-to-measured shear strength ratio of 1.0. The plot is separated by the transverse reinforcement configuration; beams in the database had either macro-synthetic fiber or deformed bar shear reinforcement, neither, or both.

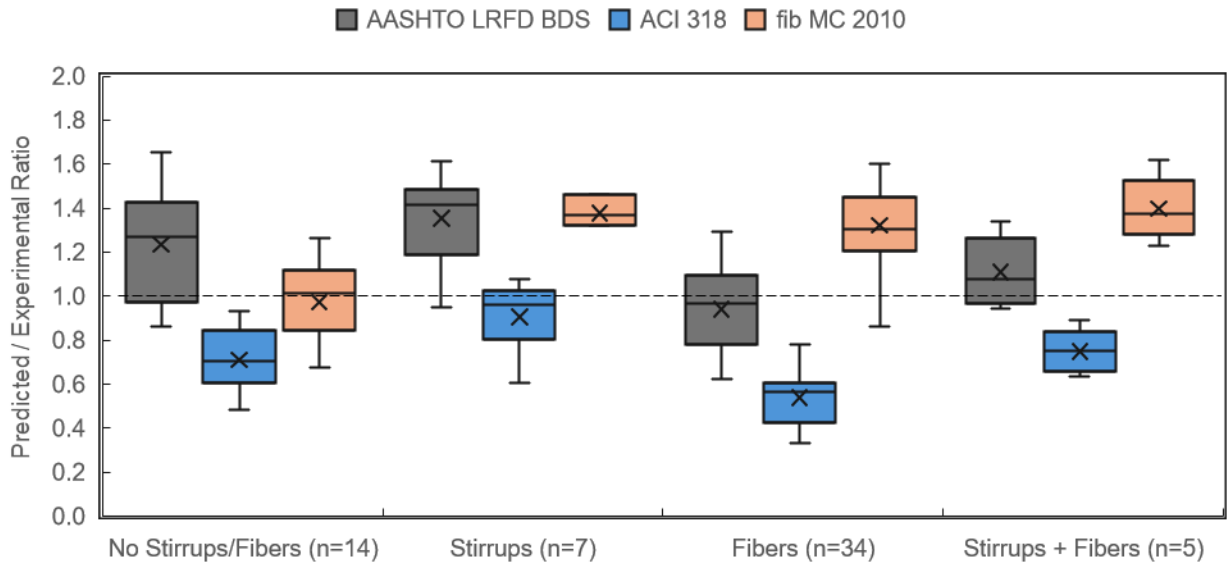

Figure 5-2. Empirical shear strength predicted-to-measured shear strength ratio for PFRC beams in the database

For the limited beam data available (9 research programs presented in Table 4-3), the AASHTO LFRD BDS predictions for shear strength were higher than the peak experimental strengths, for the beams that did not contain PFRC (mean predicted-to-measured shear strength ratio of 1.27 versus 0.96 for PFRC beams). Similarly, the ACI 318 predictions were consistently lower than the peak experimental strengths, especially for the beams that did not contain PFRC (mean predicted-to-measured shear strength ratio of 0.57 versus 0.77 for beams without fibers). Both codes neglect the contribution of the fibers and thus underpredict the shear strength of the PFRC beams (similar numerator and a smaller denominator). For the *fib* Model Code 2010, which does account for the strength contribution of the fibers, the mean predicted-to-measured shear strength ratio for beams without transverse reinforcement or fibers was 0.97 and 1.34 for beams with transverse deformed bar and/or fiber reinforcement. The reason that the shear strength of beams without transverse reinforcement and/or fibers was well predicted and beams with transverse reinforcement and/or fibers was not, is likely partially attributable to the small sample size of the available test data.

Figure 5-3a-c show the predicted panel strength from the empirical equations versus the peak shear strength of the finite element models presented in Chapter 4. The dashed line indicates a

1:1 relationship. Fig. 5-3d shows the ratio of the predicted to the numerical shear strength for the modeled panels. The dashed line indicates a predicted-to-measured shear strength ratio of 1.0.

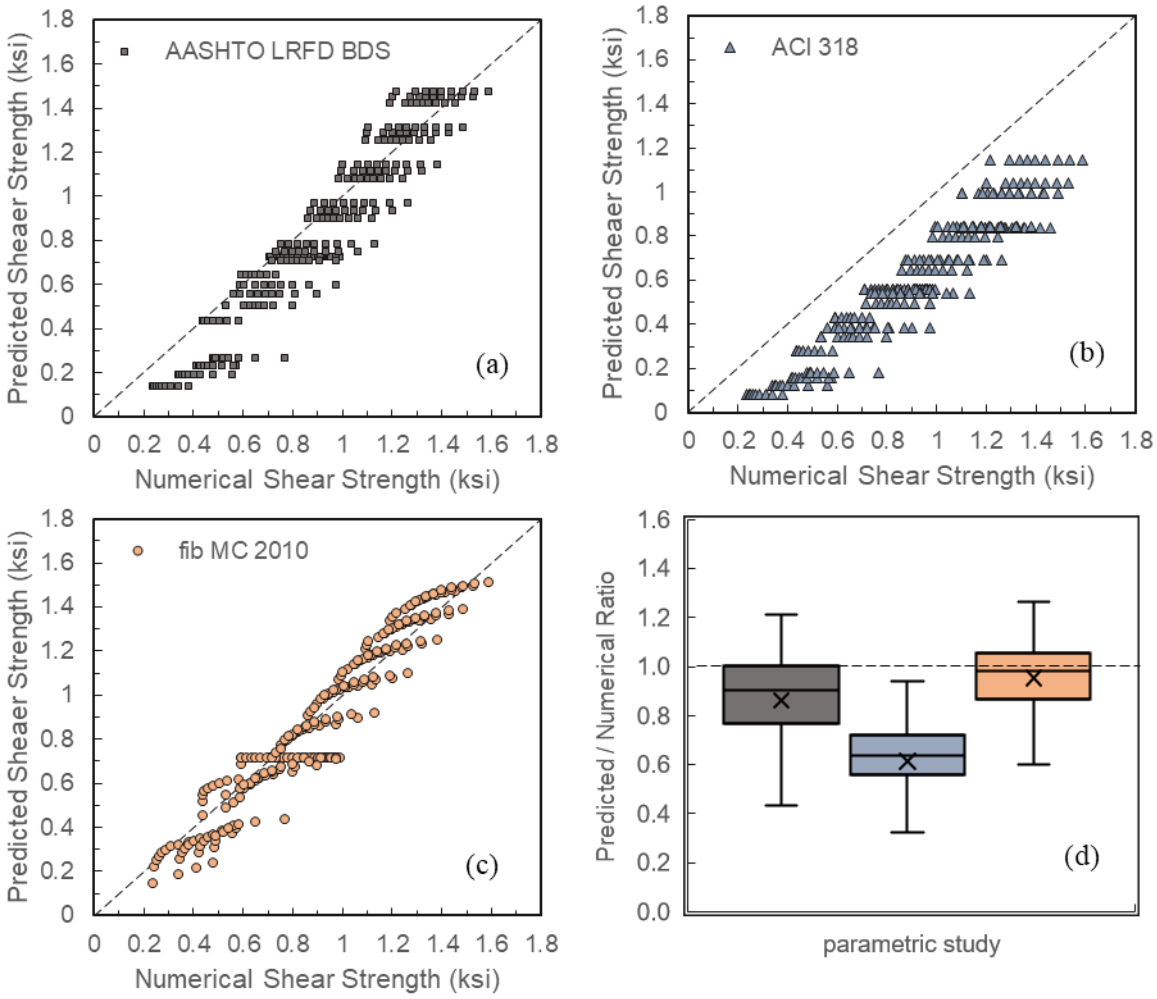

Figure 5-3. Empirical shear strength prediction for numerical PFRC panel models (a-c) predicted versus numerical shear strength (d) predicted-to-numerical shear strength ratio

In general, all three model codes conservatively estimate the shear strength of the numerical panels from the parametric study. Of the three model codes, the *fib* Model Code 2010 shear strength prediction equation matched the numerical data best with a mean predicted-to-numerical shear strength ratio of 0.94 and a COV of 0.15. The AASHTO LRFD BDS and ACI 318 equations were more conservative with mean predicted-to-numerical concrete strength ratio of 0.84 and 0.60 and COVs of 0.24 and 0.26, respectively. The inclusion of a macro-synthetic fiber contribution in the *fib* Model Code 2010 equations, and the subsequent improvement in the strength prediction for the numerical PFRC panels, can be seen visually in Figure 5-3c by observing the positively sloped, curved groupings of dots for each panel series (determined by concrete strength and transverse reinforcement ratio). This behavior is noticeably absent in Figure 5-3a and Figure 5-3b, where these groupings appear as horizontal lines.

CHAPTER 6. SUMMARY, CONCLUSIONS, AND FUTURE WORK

6.1. Summary

This research program experimentally and numerically investigated the combined use of deformed bar reinforcement and distributed macro-synthetic fibers to resist shear forces. The experimental campaign investigated the use of fiber volume fractions, transverse reinforcement ratios, and concrete mixture designs consistent with current practice. Twelve panel element specimens were tested under in-plane shear loading with transverse deformed bar reinforcement ratios, ranging from ρ_v = 0% to ρ_v = 1.14%, and macro-synthetic fiber content, ranging from V_f = 0% to V_f = 0.52% fibers by volume. The numerical modeling and parametric study extended the experimental results and explored combinations of parameters that were not, or could not be, tested experimentally. A modeling approach was calibrated using the experimental panel data, incorporating a user-defined concrete tension softening model to capture the strength contribution of the fibers. The finite element modeling approach was then validated against a database of PFRC beams from the literature, which was compiled as part of this research. The modeling approach was then used to conduct a parametric study, exploring the shear strength of PFRC panels with over 250 combinations of fiber contents, transverse reinforcement ratios, and concrete compressive strengths. The ability of existing empirical equations in model codes to predict the shear strength of PFRC structural elements was then evaluated using the experimental data available, augmented by the numerical results from the parametric study.

6.2. Conclusions

From the results of the analyses, and for the range of the parameters investigated, the following conclusions were reached:

- Macro-synthetic fibers were effective in decreasing both the maximum and average crack widths during shear loading. For the experimentally tested panels with a transverse reinforcement ratio of 0.29%, increasing the fiber volume from 0% to 0.52% reduced the maximum crack width at a shear stress of $0.13\sqrt{f'c}$ (ksi) from 0.35 mm to 0.16 mm (a roughly 50% decrease), and reduced the average crack width from 0.18 mm to 0.14 mm (22% decrease). Similar trends were observed in the parametric study.
- In the numerical models, significant increases in shear strength (i.e. 20% to 30%) were estimated when macro-synthetic fibers were utilized at addition rates greater than or equal to about 1%, irrespective of concrete compressive strength or reinforcement ratio. For the level of fiber addition tested experimentally, $V_f \leq 0.52\%$, the strength improvement in the parametric study was less than 10%. Given the potential range of experimental uncertainty, this is consistent with the results from the tested panel specimens, where no decrease in shear strength was measured with the addition of macro-synthetic fibers.
- The shear strain capacity at failure increased as fiber volume increased, however improvements depended on both the transverse reinforcement ratio and concrete compressive strength (albeit to a lesser extent). For panels without transverse deformed bar reinforcement, the influence of fiber volume fraction was the most pronounced. This is consistent with the results of Carnovale and Vecchio (2014) who found that the addition of fibers to panels containing no transverse reinforcement improved the deformation capacity of the panels.
- Based on the limited data available, the benefits of adding macro-synthetic fibers on the shear strength of structural members depends on the transverse reinforcement ratio (i.e., there is more benefit at lower transverse reinforcement ratios). This is consistent with previous

studies [e.g., Majdzadeh et al. 2006, Greenough & Nehdi 2008, Altoubat et al. 2009] that measured 20% to 40% increases in strength of macro-synthetic fiber-reinforced beams without transverse reinforcement (i.e., $\rho_v = 0\%$) or with transverse reinforcement ratios, $\rho_v = 0.14\%$.

- Of the shear strength prediction equations investigated, the *fib* Model Code 2010 equations were the most accurate for the PFRC and RC panel elements, both the experimental panels and numerical panel models. The mean predicted-to-measured shear strength ratio was 0.97 for the tested panel elements and the mean predicted-to-numerical shear strength ratio was 0.94 for the numerical panels in the parametric study. The ACI 318 equations were consistently the most conservative with predicted-to-measured shear strength ratios around 0.6.
- The AASHTO LRFD BDS concrete shear strength equations could be used to conservatively estimate the shear strength of PFRC concrete elements with fiber volumes, $V_f \leq 0.5\%$, without modification. The mean predicted-to-measured shear strength ratio was 0.87 for the tested panel elements which had a maximum fiber volume fraction of $V_f = 0.52\%$. This volume fraction represents what is currently recommended as the maximum dosage by the manufacturer for the fibers used in the tests. For higher fiber volume fractions, $V_f > 0.5\%$, the AASHTO LRFD BDS equations may be overly conservative, especially for members with the minimum transverse deformed bar reinforcement, but further testing is needed to verify.

6.3. Future work

The existing data on the behavior of macro-synthetic fiber-reinforced concrete structural elements remains limited, and significant uncertainty should be expected when forming conclusions based on any single experimental research program. From the current experimental evidence available, the addition of at least 0.5% macro-synthetic fibers by volume leads to improvements in strength on the order of 20% for beams containing equal to, or less than, the minimum shear reinforcement required by AASHTO LRD BDS [e.g., Majdzadeh et al. 2006, Greenough & Nehdi 2008, Altoubat et al. 2009]. The panel element tests performed as part of this research and in a previous study [Carnovale & Vecchio 2014] under pure shear loading, indicated no decrease in the strength of the panels with the addition of macro-synthetic fibers, but did not see the same improvements as seen in the previous beam studies. In all cases, the addition of macro-synthetic fibers decreased crack widths, both average and maximum, during loading and increased the deformability of test specimens, especially for those specimens with low levels of transverse deformed bar reinforcement ($\rho_v \leq 0.26\%$). These are positive results; however, additional test data is needed to form rational design recommendations for the combined use of macro-synthetic fibers and deformed bar reinforcement to resist shear forces.

To better understand the benefits of use of macro-synthetic fibers additional testing should focus on specimens with macro-synthetic fiber volumes, $V_f \geq 0.5\%$, and with transverse reinforcement ratios, $\rho_v \leq 0.3\%$, since the greatest benefit from fibers have been seen there. Testing that includes multiple macro-synthetic fiber types (size, shape, material, and coating) and several concrete mixture designs, optimized for workability at higher fiber volumes, would further strengthen the existing literature on the structural use of PFRC.

Additionally, a comparative study investigating the influence of test specimen (flexural beams versus shear panels) and control method (load control versus displacement control) on the influence of macro-synthetic fibers on the shear strength of reinforced concrete elements would

be informative. It is anticipated that fibers may show greater benefit for improving the flexure-shear strength of beams, versus the web-shear strength. This would be consistent with the existing literature available and may explain the different behaviors observed in this and other testing series.

REFERENCES

AASHTO (2020). AASHTO LRFD Bridge Design Specifications. American Association of State Highway and Transportation Officials, Washington, DC.

Ababneh, A., Al-Rousan, R., Alhassan, M., and Alqadami, M. (2017). Influence of synthetic fibers on the shear behavior of lightweight concrete beams. Advances in Structural Engineering, 20(11):1671–1683.

ACI (2019) Building code requirements for structural concrete (ACI 318-19) and commentary, Committee 318, American Concrete Institute Farmington Hills, MI, USA.

Alhassan, M., Al-Rousan, R., & Ababneh, A. (2017) "Flexural behavior of lightwight concrete beams encompassing various dosages of macro synthetic fibers and steel ratios." Case Studies in Constr Mat, 7: 280-293.

Altoubat, S., Yazdanbakhsh, A., and Rieder, K.-A. (2009). Shear behavior of macrosynthetic fiber-reinforced concrete beams without stirrups. ACI Materials Journal, 106(4):381.

Amin, A & Foster, S.J. (2015). Shear strength of steel fibre reinforced concrete beams with stirrups. Engineering Structures, 111: 323-332

Aoude, H., Belghiti, M., Cook, W.D., & Mitchell, D. (2012) Response of steel fiber-reinforced concrete beams with and without stirrups. ACI Struct J,109(3):359–67.

Arslan, G., Keskin, R. S. O., and Ozturk, M. (2017). Shear behaviour of polypropylene fibre-reinforced-concrete beams without stirrups. Proceedings of the Institution of Civil Engineers-Structures and Buildings, 170(3):190–198.

ASTM (2020) "C1609/C1609M Standard Test Method for Flexural Performance of Fiber-Reinforced Concrete (Using Beam With Third-Point Loading." ASTM International, West Conshohocken, PA,

ASTM (2020) D7508/D7508M "Standard Specification for Polyolefin Chopped Strands for Use in Concrete." ASTM International, West Conshohocken, PA.

ASTM (2022) "A706/A706M Standard Specification for Deformed and Plain Low-Alloy Steel Bars for Concrete Reinforcement." ASTM International, West Conshohocken, PA.

ASTM (2023) C33/C33M "Standard Specification for Concrete Aggregates." ASTM International, West Conshohocken, PA.

Bentz, E. C., Vecchio, F. J., and Collins, M. P. (2006). Simplified modified compression field theory for calculating shear strength of reinforced concrete elements. ACI structural journal, 103(4):614.

Carnovale, D. and Vecchio, F. J. (2014). Effect of fiber material and loading history on shear behavior of fiber-reinforced concrete. ACI Structural Journal, 111(5).

Carnovale, D. J. (2013). Behaviour and analysis of steel and macro-synthetic fibre reinforced concrete subjected to reversed cyclic loading: a pilot investigation. PhD thesis, University of Toronto Toronto, ON, Canada.

Chasioti, S. (2017). Hybrid steel fibre reinforced concrete in shear: from the material to the structural level. University of Toronto (Canada).

Conforti, A., Minelli, F., Tinini, A., and Plizzari, G. A. (2015). Influence of polypropylene fibre reinforcement and width-to-effective depth ratio in wide-shallow beams. Engineering Structures, 88:12–21.

Cucchiara C, Mendola LL, Papia M. (2004) Effectiveness of stirrups and steel fibres as shear reinforcement. Cement Concr Compos, 26: 777–86.

Farag, B.F. (2024) Predicting the Shear Strength of Macro-Synthetic Fiber-Reinforced Concrete using Finite Element Models. MSCE Thesis, University of Washington, Seattle, WA.

fib (2013) Model Code for Concrete Structures 2010. CEB, Lausanne, Switzerland.

Furlan Jr, S. and de Hanai, J. B. (1997). Shear behaviour of fiber reinforced concrete beams. Cement and concrete composites, 19(4):359–366.

Gaston, J. P. B. (2023). Shear behavior of macro-synthetic fiber-reinforced concrete panels. MSCE Thesis, University of Washington, Seattle, WA.

Greenough, T. and Nehdi, M. (2008). Shear behavior of fiber-reinforced self-consolidating concrete slender beams. ACI materials Journal, 105(5):468.

Haroon, S., Yazdani, N., and Tawfiq, K. (2006) "Posttensioned Anchorage Zone Enhancement with Fiber-Reinforced Concrete." J Bridge Eng, 11(5): 566-572.

Lantsoght, E. O. (2019). Database of shear experiments on steel fiber reinforced concrete beams without stirrups. Materials, 12(6):917.

Lee, S., Hassan, R., Saari, N., Mohamad, N., and Noor, N. M. (2019). Flexural behaviour of rc beams with steel and polypropylene fibres. In Journal of Physics: Conference Series, volume 1349, page 012071. IOP Publishing.

Lee, S.-C., Cho, J.-Y., and Vecchio, F. J. (2011). Diverse embedment model for steel fiberreinforced concrete in tension: Model development. ACI materials Journal, 108(5):516.

Lee, S.-C., Cho, J.-Y., and Vecchio, F. J. (2013). Simplified diverse embedment model for steel fiber-reinforced concrete elements in tension. Materials Journal, 110(4):403–412.

Li, V.C., Ward, R., & Hamza, A.M. (1992) "Steel and Synthetic Fibers as Shear Reinforcement." ACI Mat J, 89(5): 499-508.

Li, V.C., Mishra, D.K., Naaman, A.E., Wight, J.K., LaFave, J.M., Wu, H., & Inada, Y. (1994) "On the Shear Behavior of Engineered Cementitious Composites." Advn Cem Bas Mat, 1994(1): 142-149.Lim, C. N. (2006). Flexural Behavior of Steel Fiber Reinforced Concrete (SFRC). PhD thesis, Universiti Teknologi Malaysia.

Majdzadeh, F., Soleimani, S. M., and Banthia, N. (2006). Shear strength of reinforced concrete beams with a fiber concrete matrix. Canadian Journal of Civil Engineering, 33(6):726–734.

Mansur, M., Ong, K., and Paramasivam, P. (1986). Shear strength of fibrous concrete beams without stirrups. Journal of structural engineering, 112(9):2066–2079.

Murad, Y. and Abdel-Jabbar, H. (2022). Shear behavior of rc beams prepared with basalt and polypropylene fibers. Case Studies in Construction Materials, 16:e00835.

Navas, F. O., Navarro-Gregori, J., Herdocia, G. L., Serna, P., and Cuenca, E. (2018). An experimental study on the shear behaviour of reinforced concrete beams with macrosynthetic fibres. Construction and Building Materials, 169:888–899.

Sahoo, D. R., Maran, K., and Kumar, A. (2015). Effect of steel and synthetic fibers on shear strength of rc beams without shear stirrups. Construction and Building Materials, 83:150–158.

Shah, S. P., & Rangan, B. V. (1971). Fiber reinforced concrete properties. ACI Journal Proceedings, 68(2). https://doi.org/10.14359/11299

Susetyo, J. (2009). Fibre reinforcement for shrinkage crack control in prestressed, precast segmental bridges. PhD thesis, University of Toronto.

Swamy, R. N., & Bahia, H. M. (1985). The effectiveness of steel fibers as shear reinforcement. Concrete International.

Vecchio, F. J. and Collins, M. P. (1986). The modified compression-field theory for reinforced concrete elements subjected to shear. ACI J., 83(2):219–231.

Voo, J. Y. L. and Foster, S. J. (2003). Variable engagement model for the design of fibre reinforced concrete structures.

Wong, P., Vecchio, F., and Trommels, H. (2013). Vector2 & formworks user's manual second edition. University of Toronto, Canada.

Zhang, H., Calvi, P. M., Lehman, D., Kuder, K., & Roeder, C. (2020). Response of recycled coarse aggregate concrete subjected to pure shear. Journal of Structural Engineering, 146(5). https://doi.org/10.1061/(asce)st.1943-541x.0002620

Zhang, Z. (2020). Finite Element Modelling of Ultra-High Performance Fibre Reinforced Concrete. University of Toronto (Canada).